Estimating Asian terrestrial carbon fluxes from CONTRAIL aircraft and surface CO_2 observations for the period 2006 to 2010

H. F. Zhang[1,2], B. Z. Chen[1,*], I. T. van der Laan−Luijkx[3], T. Machida[4], H. Matsueda[5], Y. Sawa[5], Y. Fukuyama[6], C. Labuschagne[7], R. Langenfelds[8], M. van der Schoot[8], G. Xu[1,2], J. W. Yan[1,2], L. X. Zhou[9], P. P. Tans[10], W. Peters[3,11]

[1] State Key Laboratory of Resources and Environment Information System, Institute of geographic Sciences and Natural Resources Research, Chinese Academy of Sciences, Beijing 100101, China

[2] University of Chinese Academy of Sciences, Beijing 100049, China

[3] Department of Meteorology and Air Quality (MAQ), Wageningen University, Droevendaalsesteeg 3a, NL−6700 PB, Wageningen, The Netherlands

[4] Center for Global Environmental Research, National Institute for Environmental Studies, Tsukuba, Japan

[5] Geochemical Research Department, Meteorological Research Institute, Tsukuba, Japan

[6] Atmospheric Environment Division, Global Environment and Marine Department, Japan Meteorological Agency

[7] South African Weather Service, P.O. Box 320, Stellenbosch, 7599 South Africa

[8] Centre for Australian Weather and Climate Research/CSIRO Marine and Atmospheric Research, Aspendale, Victoria, Australia

[9] Key Laboratory for Atmospheric Chemistry of China Meteorological Administration, Research Institute of Atmospheric Composition of Chinese Academy of Meteorological Sciences, Beijing 100081, China

[10] Earth System Research Laboratory, National Oceanographic and Atmospheric Administration, Boulder, Colorado 80305, USA

[11] Centre for Isotope Research, Groningen, The Netherlands

Correspondence to: B. Z. Chen (baozhang.chen@igsnrr.ac.cn)

Revised version to *Atmos. Chem. Phys.*

Abstract

Current estimates of the terrestrial carbon fluxes in Asia ("Asia" refers to lands as far west as the Urals and is divided into Boreal Eurasia, Temperate Eurasia and tropical Asia based on TransCom regions) show large uncertainties particularly in the boreal and mid-latitudes and in China. In this paper, we present an updated carbon flux estimate for Asia by introducing aircraft CO_2 measurements from the CONTRAIL (Comprehensive Observation Network for Trace gases by Airline) program into an inversion modeling system based on the CarbonTracker framework. We estimated the averaged annual total Asian terrestrial land CO_2 sink was about –1.56 Pg C yr^{-1} over the period 2006-2010, which offsets about one-third of the fossil fuel emission from Asia (+4.15 Pg C yr^{-1}). The uncertainty of the terrestrial uptake estimate was derived from a set of sensitivity tests and ranged from –1.07 to –1.80 Pg C yr^{-1}, comparable to the formal Gaussian error of ±1.18 Pg C yr^{-1} (1-sigma). The largest sink was found in forests, predominantly in coniferous forests (–0.64 Pg C yr^{-1}) and mixed forests (–0.14 Pg C yr^{-1}); and the second and third large carbon sinks were found in grass/shrub lands and crop lands, accounting for –0.44 Pg C yr^{-1} and –0.20 Pg C yr^{-1}, respectively. The peak-to-peak amplitude of inter-annual variability (IAV) was 0.57 Pg C yr^{-1} ranging from –1.71 Pg C yr^{-1} to –2.28 Pg C yr^{-1}. The IAV analysis reveals that the Asian CO_2 sink was sensitive to climate variations, with the lowest uptake in 2010 concurrent with a summer flood & autumn drought and the largest CO_2 sink in 2009 owing to favorable temperature and plentiful precipitation conditions. We also found the inclusion of the CONTRAIL data in the inversion modeling system reduced the uncertainty by 11% over the whole Asian region, with a large reduction in the southeast of Boreal Eurasia, southeast of Temperate Eurasia and most Tropical Asian areas.

1 Introduction

The concentration of carbon dioxide (CO_2) has been increasing steadily in the atmosphere since the industrial revolution, which is considered to be very likely responsible for the largest contribution of the climate warming (Huber and Knutti, 2011; Peters et al., 2011). Knowledge of the terrestrial carbon sources and sinks is critically important for understanding and projecting the future atmospheric CO_2 levels and climate change. The global terrestrial ecosystems absorbed about 1-3 Pg carbon every year during the 2000s, with obvious interannual variations, offsetting 10-40% of the anthropogenic emissions (Le Quéré et al., 2009; Maki et al., 2010; Saeki et al., 2013). However, estimates of the terrestrial carbon balance vary considerably when considering continental scales and smaller, as well as when estimating the CO_2 seasonal and inter-annual variability (Houghton, 2007; Peylin et al., 2013).

Asia, as one of the biggest northern hemisphere terrestrial carbon sinks, has a significant impact on the global carbon budget (Jiang et al., 2013; Patra et al., 2012; Piao et al., 2009; Piao et al., 2012; Peylin et al., 2013; Yu et al., 2013). It is estimated that Asian ecosystems contribute over 50% of the global net terrestrial ecosystem exchange (Maksyutov et al., 2003) and their future balance is thought to be a great uncertainty source for the global carbon budget (Ichii et al., 2013; Oikawa and Ito, 2001). Even though the importance of the Asian ecosystems is increasingly recognized and many efforts have been carried out to estimate the Asian terrestrial carbon sources and sinks, they still remain poorly quantified (Ito, 2008; Patra et al., 2013; Patra et al., 2012; Piao et al., 2011). One reason is that a steep rise of fossil fuel emissions in most Asian countries has imposed large influences on the Asian CO_2 balance and leads to an increased variability of the regional carbon cycle (Francey et al., 2013; Le Quere et al., 2009; Patra et al., 2013; Patra et al., 2011; Raupach et al., 2007). In addition, quick land-use change and climate change have likely increased the variability in the Asian terrestrial carbon balance (Cao et al., 2003; Patra et al., 2011; Yu et al., 2013). All these together make it challenging to accurately estimate of

CO_2 fluxes of the Asia ecosystems.

Currently two approaches are commonly used to estimate CO_2 fluxes at regional to global scales: the so-called "bottom-up" and "top-down" methods. The bottom-up approach is based on local data or field measurements to retrieve the carbon fluxes, including direct measurements (Chen et al., 2012; Clark et al., 2001; Fang et al., 2001; Mizoguchi et al., 2009; Takahashi et al., 1999) and ecosystem modeling (Chen et al., 2007; Fan et al., 2012; Randall et al., 1996; Randerson et al., 1997; Sellers et al., 1986; Sellers et al., 1996). The top-down method uses atmospheric mole fraction data to derive the CO_2 sink/source information. As one of the important "top-down" approaches, atmospheric inversion modeling has been well developed and widely applied (Baker et al., 2006; Chevallier and O'Dell, 2013; Deng et al., 2007; Gurney et al., 2003; Gurney et al., 2004), and has shown to be particularly successful in estimating regional carbon flux for regions rich in atmospheric CO_2 observations like North America and Europe (Broquet et al., 2013; Deng et al., 2007; Peters et al., 2007; Peters et al., 2010; Peylin et al., 2013; Peylin et al., 2005; Rivier et al., 2011, 2010). However, estimating Asian CO_2 surface fluxes with inversion modeling remains challenging, and the inverted Asian CO_2 fluxes still exhibit a large uncertainty partly because of lack of surface CO_2 observations. For example, in the TransCom3 annual mean control inversion, Gurney*, et al.* (2003) used a set of 17 models to estimate the carbon fluxes and obtained different results for the Asian biospheric CO_2 budget, ranging from a large CO_2 source of +1.00±0.61 Pg C yr^{-1} to a large sink of −1.50±0.67 Pg C yr^{-1} for the year 1992-1996. In the RECCAP (REgional Carbon Cycle Assessment and Processes) project, Piao*, et al.* (2012) presented the carbon balance of terrestrial ecosystems in East Asia from eight inversions during 1990-2009. The results from these eight inversion models also show disagreement: six models estimate a net CO_2 uptake with the highest net carbon sink of −0.997 Pg C yr^{-1}, while two models show a net CO_2 source with the largest net carbon emission of +0.416 Pg C yr^{-1} in East Asia. The important role of the sparse observational network was demonstrated by Maki, et al. (2010), who reported a large Asian land sink of

−1.17±0.50 Pg C yr^{-1} or much smaller sink of −0.65±0.49 Pg C yr^{-1} over the Asian region depending on which set of observations was included in the same inversion system. This situation suggests that a more accurate inverted estimate of the surface CO_2 flux is urgently required in Asia, and the ability to ingest as much observational data as possible is the key.

To expand the number of CO_2 observation data points, the aircraft project of CONTRAIL has been operated to measure CO_2 concentration onboard passenger flights since 2005, and has produced a large coverage of *in situ* CO_2 data ranging over various latitudes, longitudes, and altitudes (Machida et al., 2008; Matsueda et al., 2008). Huge amounts of CONTRAIL measurements have been made and have already successfully been used to constrain surface flux estimates (Niwa et al., 2012; Niwa et al., 2011; Patra et al., 2011). Patra et al. (2011) reported the added value of CONTRAIL data to inform on tropical Asian carbon fluxes, as their signals are transported rapidly to the free troposphere over the west Pacific.

In this study, we also used the CONTRAIL CO_2 observations (http://www.cger.nies.go.jp/contrail/) together with a global network of surface observations to estimate the Asian weekly net ecosystem exchange of CO_2 (NEE) during the period 2006-2010. Our inversion model is the state-of-the-art CO_2 data assimilation system CTDAS (CarbonTracker Data Assimilation Shell, http://carbontracker.eu/ctdas/). Our work complements previous inverse modeling studies as it: (1) presents the inverted CO_2 results of Asian weekly net ecosystem exchange not shown previously; (2) uses surface observations not available in an earlier top-down exercises; (3) assimilates the continuous CO_2 observation from a number of Asian continental sites for the first time; (4) includes extra free tropospheric CO_2 observations to further constrain the estimation; (5) uses a two-way atmospheric transport model TM5 (Krol et al., 2005) with higher horizontal resolution than previous global CO_2 data assimilation studies that zoomed in Asia (at 1×1 degree grid over Asia while globally at a 2×3 degree resolutions, see Figure 1).

This paper is organized as follows. Methods and materials are described in Section 2,

the inferred Asian land flux and its temporal-spatial variations are presented in Section 3. To examine the impact of CONTRAIL data on Asian flux estimation, we also compared inversion results with and without CONTRAIL data during 2006-2010. In Section 4, we compare our inverted Asian surface fluxes with previous findings and discuss our estimation uncertainty estimates and future directions. Note that the "Asia" refers to lands as far west as the Urals, and it is further divided into Boreal Eurasia, Temperate Eurasia and tropical Asia based on TransCom regions (Gurney et al., 2002; Gurney et al., 2003) (see small inset in the bottom left corner of Figure 2).

2 Methods and datasets

2.1 The atmospheric inversion model (CTDAS)

The atmospheric inversion model CTDAS was developed by NOAA-ESRL (National Oceanic and Atmospheric Administration's Earth System Research Laboratory) & Wageningen University, the Netherlands. Previous versions of the system have been applied successfully in North America and Europe (Masarie et al., 2011; Peters et al., 2007; Peters et al., 2010). CTDAS was designed to estimate net CO_2 terrestrial and oceanic surface fluxes by integrating atmospheric CO_2 concentration measurements, a global transport model, and a Bayesian synthesis technique that minimizes the difference between the simulated and observed CO_2 concentrations. The first step is the forecast of the atmospheric CO_2 concentrations using the transport model TM5 (Krol et al., 2005) with a global resolution of 3×2 degrees and 1×1 degrees over Asia (see figure 1), driven by meteorological data of the European Centre for Medium-Range Weather Forecasts (ECMWF) and four separate sets of bottom-up fluxes (details are presented in the Section 2.2). Secondly, these forecasted four-dimensional (4-D) concentrations (x, y, z, t) are sampled with the observed atmospheric CO_2 mole fractions at the location and time of the measurements, which are then compared. The difference between the observed and simulated CO_2 concentrations is minimized. This minimization of the concentration differences in CTDAS is done by tuning a set of linear scaling factors which are applied to find the set of sources and sinks that most closely match the observed CO_2 concentration in

the atmosphere.

As described in Peters *et al.* (2007), four a-priori and imposed CO_2 fluxes integrate in CTDAS to instantaneous CO_2 fluxes F(x, y, t) as follows:

$$F(x,y,t) = \lambda_r F_{bio}(x,y,t) + \lambda_r F_{oce}(x,y,t) + F_{ff}(x,y,t) + F_{fire}(x,y,t) \quad (1)$$

where F_{bio} and F_{oce} are 3-hourly, 1°×1° a-priori terrestrial biosphere and ocean fluxes, respectively; F_{ff} and F_{fire} are monthly 1°×1° prescribed fossil fuel and fire emissions, and λ_r is a set of weekly scaling factors, and each scaling factor is associated with a particular region of the global domain that is divided into 11 land and 30 ocean regions according to climate zone and continent. Nineteen ecosystem types (Olson et al., 1985) (Figure 2a) have been considered in each of 11 global land areas (Gurney et al., 2002), dividing the globe into 239 regions (239 = 11 land × 19 ecosystem types + 30 ocean regions). The actual region number assimilated in this system is 156, after excluding 83 regions which associated with a non-existing ecosystem (such as "snowy conifers" in Africa). The corresponding scaling factors have been estimated as the final product of CTDAS, and have been applied to obtain the terrestrial biosphere and ocean fluxes at the ecosystem and ocean basin scale by multiplying them with the a-priori fluxes. The adjusted fluxes are then put into the transport model to produce an optimized 4-D CO_2 concentration distribution.

2.2 A priori CO_2 flux data set

In CTDAS, four types of CO_2 surface fluxes are considered: (1) the a-priori estimates of the oceanic CO_2 exchange are based on the air-sea CO_2 partial pressure differences from ocean inversions results (Jacobson et al., 2007). These air-sea partial pressure differences are combined with a gas transfer velocity computed from wind speeds in the atmospheric transport model to compute fluxes of carbon dioxide across the sea surface every 3 hours; (2) the a-priori terrestrial biosphere CO_2 fluxes are from GFED2 (Global Fire Emissions Database version 2), which is derived from the Carnegie-Ames Stanford Approach (CASA) biogeochemical modeling system (Van

der Werf et al., 2006). A monthly varying NEE flux ($NEE = R_e - GPP$) was constructed from two flux components: gross primary production (GPP) and ecosystem respiration (R_e), and interpolated to 3-hourly net land surface fluxes using a simple temperature Q_{10} relationship assuming a global Q_{10} value of 1.5 for respiration, and a linear scaling of photosynthesis with solar radiation. (3) The imposed fossil fuel emission estimates from the global total fossil fuel emission of the CDIAC (Carbon Dioxide Information and Analysis Center) (Marland et al., 2003) were spatially and temporally interpolated following the EDGAR (Emission Database for Global Atmospheric Research) database (Boden et al., 2011; Commission, 2009; Olivier and Berdowski, 2001; Thoning et al., 1989); (4) the biomass burning emissions are from the GFED2, which combines monthly burned area information observed from satellites (Giglio et al., 2006) with the CASA biogeochemical model. Fire emissions in GFED2 are available only up to 2008, so for 2009 and 2010 we use a climatologically of monthly averages of the previous decade. Note that GFED3 (and now even GFED4) is available for quite a few years, and offers higher spatial resolutions in biomass burning emissions which are attractive for model simulation. But it uses a different product for the satellite observed NDVI and fPAR (MODIS instead of AVHRR) which causes a different seasonality in the biosphere fluxes which are calculated alongside the fire emissions in GFED, with a less realistic amplitude. Since this amplitude of the seasonal biosphere is important to us, we did not update to this new GFED3 product. We also tested the GFED4 data with SIBCASA to make a new dataset of fire estimates but our analyses showed that the impact of using GFED4 versus GFED2 on estimated Asia fluxes is very weak.

2.3 Atmospheric CO_2 observations

For this study, two sets of atmospheric CO_2 observation data were assimilated: (1) surface CO_2 observations distributed by NOAA-ESRL (http://www.esrl.noaa.gov/gmd/ccgg/obspack/, data version 1.0.2) and by the WDCGG (World Data Centre for Greenhouse Gases, http://ds.data.jma.go.jp/gmd/wdcgg/) for the period 2006-2010 (the Asian surface site

information is summarized in Figure 2a and the global surface sites *are in Supporting Information Appendix A*). Individual time series in this surface set were provided by many individual PIs which we kindly acknowledge; (2) for the free tropospheric CO_2 observation, we use the aircraft measurements derived from the CONTRAIL project for the period 2006-2010 (see Figure 2b).

A summary of Asian surface sites used in this study is shown in Table 1 and Figure 2a for a reference. There are fourteen surface sites with over 7,957 observations located in Asia, including 10 surface flask observations and 4 surface continuous sites. These surface CO_2 mole fraction data used in this study are all calibrated against the same CO_2 standard (WMO-X2007). For most of the continuous sampling sites at the surface, we derived a daily averaged afternoon CO_2 concentration (12:00-16:00, Local time) for each day from the time series, while at mountain-top sites we construct an average based on nighttime hours (0:00-4:00, Local time) to reduce local influence and compare modeled with observed values only for well mixed conditions.

In our assimilation system, we also use free tropospheric continuous aircraft measurements from the CONTRAIL program (Machida et al., 2008; Matsueda et al., 2008) to constrain the inverted CO_2 flux. Note that stratospheric CONTRAIL CO_2 data were not included into the CTDAS for the stratospheric observation had a seasonal phase shifting and its smaller amplitude was hard to compare to the tropospheric measurements (Sawa et al., 2008). A summary of the CONTRAIL aircraft measurements is presented in Table 2 and Figure 2b. The CONTRAIL aircraft data are reported on the NIES 09 CO_2 scale, which are lower than the WMO−X2007 CO_2 scale by 0.07 ppm at around 360 ppm and consistent in the range between 380 and 400 ppm (Machida et al., 2011). Thus the CONTRAIL CO_2 data sets are comparable to surface data well. We follow the method from Niwa*, et al.* (2012) to divide the data into 4 vertical bins (575−625, 465−525, 375−425, 225−275 hPa) from ascending & descending profiles and one vertical bin (225−275 hPa) from level cruising. We also divide CONTRAIL data into 42 horizontal bins/regions (Figure 2b), which amounts to a total of 65 bins. Before daily averaging the CONTRAIL

measurements for each 65 regional/vertical bins，we pre-process the aircraft data to obtain free troposphere CO_2 values by filtering out of the stratospheric CO_2 data using the threshold of potential vorticity (PV) > 2 PVU (1 PVU= 10^{-6} m^2 s^{-1} K kg^{-1}), in which PV is calculated from the TM5 (ECMWF temperature, pressure and wind fields) (Sawa et al., 2008). A total number of 10,467 CO_2 aircraft observations over Asia have been used during January 2006 to December 2010 in our inversion.

2.4 Sensitivity experiments and Uncertainty Estimation

Because the Gaussian uncertainties strongly depends on choices of prior errors in CTDAS, the formal covariance estimates for each week of optimization only reflect the random component of the inversion problem rather than a characterization of the true uncertainties of the estimated CO_2 flux. As an alternative, we performed a set of sensitivity experiments to obtain a more representative spread in the flux estimates and complement the formal Gaussian uncertainty estimates. We take different plausible alternative settings in CTDAS to design a more comprehensive sensitivity tests, and use the minimum and maximum flux inferred in these experiments to present the range of the true flux we expected. Six inversions were performed to investigate the uncertainty span in this study:

Case 1: prior flux as in section 2.2 + observations as in section 2.3 + TM5 transport model runs at global $3^{\circ}\times2^{\circ}$ and a $1^{\circ}\times1^{\circ}$ nested grid over Asia. This is the base simulation (quoted as Surface-CONTRAIL) which performs the best assimilation on CO_2 source/sink and its results are used to analyze the 5-year carbon balance in this study.

Case 2: same as Case 1, but excluding CONTRAIL observations. We use these results (quoted as Surface-Only) to examine the impact of CONTRAIL data on Asian flux estimates by comparison with Case 1.

Case 3: Like Case 1, but CTDAS runs with the updated fossil fuel emissions based on Wang, *et al.* (2012) over China; This simulation is meant to partly address the impact of uncertainty in fossil fuel emissions over the region as suggested by (Francey et al.,

2013)

Case 4: Like Case 1, but CTDAS runs based on 110% of prior biosphere flux derived from CASA-GFED2;

Case 5: Like Case 2, but the TM5 transport model is used at global 6◦×4◦ without nested grids. This tests the impact of model resolution;

Case 6: Like case 2, but replacing the underlying land use map with MODIS data (Friedl et al., 2002) and keeping the number of ecoregions unchanged. The MODIS land use maps can be found in SI Appendix C.

The Cases 1 and 2 span the period 2006-2010 (2000-2005 were discarded as spin-up), while the other sensitivity experiments were done from 2008 to 2010 only when the observational coverage was best. In generally, the simulations of these six sensitivity tests investigate most variations in the components of the assimilation framework: prior fluxes, observation available, ecoregion map, fossil fuel emissions and transport, and give alternative choices for the main components of the system. The sensitivity results are summarized in the Table 3 and further discussed in the next section.

3 Results

We will from here on refer to carbon sinks with a negative sign, source with a positive, and will include the sign also when discussing anomalies (positive = less uptake or larger source, negative = more uptake or smaller source). We describe the results mainly over Asia (global flux estimates can be found in SI Appendix B), where we expected the CONTRAIL data to provide the additional constraints. Note that the results of Case 1 are analyzed as the best assimilation for the period of 2006-2010 in this study.

3.1 CO_2 concentration simulations

First we checked the accuracy of the model simulation using the surface CO_2 concentration observations and CONTRAIL aircraft CO_2 measurements. Figure 3a shows the comparison of modeled (both prior and posterior) CO_2 concentration with

measurements at the discrete surface site of Mt. Waliguan (WLG, located at 36.29° N, 100.90° E). Note that the prior CO_2 concentrations here are not really based on a-priori fluxes only, as they are a forecast started from the CO_2 mixing ratio field that contains all the already optimized fluxes (1,…, n-1) that occurred before the current cycle of the data assimilation system (n). So these prior mole fractions only contain five weeks of recent un-optimized fluxes and constitute our 'first-guess' of atmospheric CO_2 for each site. For the WLG site, the comparison of the surface CO_2 time series shows that the modeled (both prior and posterior) CO_2 concentration is in general agreement with observed data during the period 2006-2010 (correlation coefficient R=0.87), although the modeled result still could not adequately reproduce all the observed CO_2 seasonal variations. The posterior annual model-observation mismatch of this distribution is −0.10±1.25, with 0.07±1.50 ppm bias for the summer period (June-July-August) and 0.02±0.80 ppm bias for the winter period (December-January-February). Over the full study period, the WLG modeled mole fractions exhibit good agreement with the observed CO_2 time series and the changes in inferred mixing ratios/flux are within the specified uncertainties in our inversion system, an important prerequisite for a good flux estimate.

We also checked the inversion performance in the free troposphere in addition to the surface CO_2. Figures 3b, 3c and 3d show the comparison between measured and modeled (both prior and posterior) mixing ratios in the free troposphere during the period 2006-2010 in the region covering 136-144°N, 32-40°E for 3 vertical bins (475–525, 375–425, 225–275 hPa). The observed vertical CO_2 patterns were reasonably reproduced by our model, with high correlation coefficient (R = 0.95, 0.94 and 0.93 for 475–525, 375–425, 225–275 hPa, respectively) between CONTRAIL and modeled CO_2. The observed low vertical gradients for flight sections in 3 vertical bins (475–525, 375–425, 225–275 hPa) at northern mid-latitudes (32-40°E) were well captured by the model (both prior and posterior), indicating the transport model can reasonably produce the vertical structure of observations. We also found that the observed CO_2 concentration profiles were modeled better after assimilation than

before (modelled –observed = −0.01±1.18 ppm for a-priori and 0.05±1.25 ppm for posterior), although our inverted (posterior) mole fractions still could not adequately reproduce the high values in winter (December-January-February) and the low values in summer (June-July-August). This mismatch of CO_2 seasonal amplitude suggests that our inverted (posterior) CO_2 surface fluxes do not catch the peak of terrestrial carbon exchange well. Previous studies have also found this seasonal mismatch, which may correlate with atmospheric transport, and has already been identified as a shortcoming in most inversions (Peylin et al., 2013; Saeki et al., 2013; Stephens et al., 2007; Yang et al., 2007). Overall, the agreement between the modeled and measurements is fairly good and consistent with previously known behavior in the CarbonTracker systems, derived mostly from North American and European continuous sites.

3.2 Inverted Asian terrestrial CO_2 flux

3.2.1 Five-year mean

During the period 2006-2010, we found a mean net terrestrial land carbon uptake (a posteriori) in Asia of −1.56 Pg C yr^{-1}, consisting of −2.02 Pg C yr^{-1} uptake by the terrestrial biosphere and +0.47 Pg C yr^{-1} release by biomass burning (fire) emission (Table 5). This terrestrial uptake compensates 38% of the estimated +4.15 Pg C yr^{-1} CO_2 emissions from fossil fuel burning and cement manufacturing in Asia. An uncertainty analysis for the Asian terrestrial CO_2 uptake derived from a set of sensitivity experiments has been conducted and put the estimated sink ranging from −1.07 to −1.80 Pg C yr^{-1} (Table 3), while the 1-sigma of the formal Gaussian uncertainty estimate is ±1.18 Pg C yr^{-1} (Table 5). The estimated Asian net terrestrial CO_2 sink is further partitioned into: a −1.02 Pg C yr^{-1} carbon sink in Boreal Eurasia and a −0.68 Pg C yr^{-1} carbon sink in Temperate Eurasia, whereas a +0.15 Pg C yr^{-1} CO_2 source in tropical Asia.

The annual mean spatial distribution of net terrestrial carbon uptake over Asia is shown in Figure 4. Note that the estimated fluxes include terrestrial fluxes and

biomass burning sources but exclude fossil fuel emissions. Most Asian regions were natural carbon sinks over the studied period, with strongest carbon uptake in the middle and high latitudes of the Northern Hemispheric part of Asia, while the low-latitude region releases CO_2 to the atmosphere. This flux distribution pattern is quite consistent with previous findings that northern temperate and high latitude ecosystems were large sinks (Hayes et al., 2011) and tropical land regions were carbon sources (Gurney et al., 2003).

The aggregated terrestrial CO_2 fluxes for 19 different ecosystems (Figure 2a) averaged over the period 2006-2010 are shown in Table 4 and Figure 5 (see Case 1). The majority of the carbon sink was found in the regions dominated by forests, crops and grass/shrubs. The largest uptake is by the forests with a mean sink of −0.77 Pg C yr^{-1}, 83% of which (−0.64 Pg C yr^{-1}) was taken up by conifer forests and 18% of which (−0.14 Pg C yr^{-1}) by mixed forest, whereas the tropical forests released CO_2 by the amount of +0.08 Pg C yr^{-1}. The estimated flux by CTDAS in the Asian cropland ecosystems was −0.20 Pg C yr^{-1}, with the largest crop carbon sink located in Temperate Eurasia (−0.17 Pg C yr^{-1}). The grass/shrub lands in Asia absorbed −0.44 Pg C yr^{-1}, with most of these grass/shrub sinks located in Temperate Eurasia (−0.36 Pg C yr^{-1}). Other land-cover types (e.g. wetland, semi tundra and so on) sequestered about −0.15 Pg C yr^{-1} (10% of total) over Asian regions. This suggests that according to our model, many ecosystems contributed to Asian CO_2 sinks, highlighting the complexity of the northern hemispheric total sinks.

3.2.2 Seasonal variability

Figure 6 shows the *prior* and *posterior* seasonal cycles of CO_2 fluxes for the Asia region and its three sub-regions as well as their Gaussian uncertainties. The seasonal amplitude in Boreal Eurasia as shown in Figure 6b proves to be the major contributor to the seasonal signal in Asia (Figure 6a). The large uptake of Eurasia Boreal occurs in summer and the large differences between the prior and the posterior fluxes are also found in the summer growing season, indicating the surface observation network and

CONTRAIL data largely affect the estimated fluxes. Our monthly variability is very close to changes in Eurasia Boreal presented by Gurney, et al. (2004). In Figure 6c, the seasonal pattern for the Eurasia temperate region shows a comparable pattern to Eurasia Boreal, but with a smaller seasonal magnitude. And the adjustments of the *prior* flux in spring and summer are also smaller. The largest CO_2 uptake in Eurasia Temperate subregion, however, is shifted from July to August compared to Boreal Eurasia, suggesting that a phase shift in the growing season occurred here with the highest CO_2 sink occurring later in the year. This seasonal cycle is slightly different from that reported by Gurney, et al. (2004), but shows a nice agreement with the seasonal dynamics of Niwa, et al. (2012) in the Southern Temperate Asia region, and of Patra et al. (2011) in the Northwest Asia region. In Tropical Asia (Figure 6d), the seasonal variation is very different from other Asian subregions characterized by a weak CO_2 uptake peak in August-October and much smaller carbon release in May-July. Overall, the *posterior* uncertainty reduction for the period 2006-2010 was about 25% in Asia, with the largest uncertainty remaining in the summer, suggesting that our model may not fully capture the biosphere sink signal in the growing season.

3.2.3 Interannual variability (IAV)

Figure 7 shows the estimated annual cumulative net ecosystem exchange in Asia during 2006-2010 as well as its anomaly with weekly intervals. Here, the biomass burning and fossil fuel emissions are excluded, and only the fluxes from respiration and photosynthesis are shown, because biomass burning emissions have large interannual variability, especially for Tropical Asia.

The coefficient of IAV (IAV = standard deviation/mean) in Asian land carbon flux is 0.12, with a peak-to-peak amplitude of 0.57 Pg C yr^{-1} (amplitude = smallest – largest CO_2 sink), ranging from the smallest carbon uptake of −1.71 Pg C yr^{-1} in 2010 and the largest CO_2 sink of −2.28 Pg C yr^{-1} in 2009. As has been noted in many other studies (Gurney et al., 2008; Gurney et al., 2004; Mohammat et al., 2012; Patra et al., 2011; Peters et al., 2007; Peters et al., 2010; Yu et al., 2013), the IAV of the carbon flux

strongly correlates with climate factors, such as air temperature, precipitation and moistures.

The year 2010 stands out as a particularly low uptake year in Asia, with a reduction of terrestrial uptake of 0.31 Pg C yr^{-1} compared to the five-year mean. This reduction phenomenon mainly appeared in Temperate Eurasia and Tropical Asia, leading to a 0.25 Pg C yr^{-1} (35% reduction) and 0.04 Pg C yr^{-1} flux anomalies (24% reduction) in their corresponding regions. In 2010, Asia experienced a set of anomalous climate events. For example, Temperate Eurasia experienced a severe spring/autumn drought, a heavy summer flood and a heat wave occurred in 2010 (NationalClimateCenter, 2011). From Figure 7b, we can see that 2010 did not show large anomalies until after the spring growing season. As anomalous climate appeared, the summer flood and autumn drought were identified as dominant climatic factors controlling vegetation growth and exhibiting a significant correlation with the land carbon sink, particularly in the croplands, grasslands and forests of Temperate Eurasia. In the end, 2010 only showed –1.71 Pg C yr^{-1} biospheric CO_2 uptakes (excluding fires) by the end of the year.

In contrast to 2010, the year of 2009 had the strongest carbon sink for the study period, with much stronger uptake in Temperate Eurasia (−0.20 Pg C yr^{-1} anomaly, 28% increase in CO_2 uptake) as well as Boreal Eurasia (−0.05 Pg C yr^{-1} anomaly, 4% uptake increase compared to the five-year mean). It can be seen that 2009 started with a lower-than-average release of carbon in the first 4 months (17 weeks) of the year amounting to +0.28 Pg C yr^{-1} compared to the five-year average of +0.45 Pg C yr^{-1}. This variation of the Asian terrestrial carbon sink in the spring vegetation growing season may partly relate to a higher spring temperature in 2009 which induced an earlier onset of the growing season and lead to a high vegetation productivity by extending the growing season (Mohammat et al., 2012; Richardson et al., 2009; Walther et al., 2002; Wang et al., 2011; Yu et al., 2013). From Figure 7b, 2009 shows a very high carbon uptake in the summer growing season (June-August, week 22 to 32) concurrent with favorable temperature and abundant precipitation conditions. After this summer, the vegetation productivity returned back to normal and the total

cumulative carbon sink added up to −2.28 Pg C yr^{-1} at the end of the year with −0.26 Pg C yr^{-1} extra uptake compared to the five-year mean.

3.2.4 Uncertainty Estimation

Table 3 presents the estimated annual mean NEE across the alternative sensitivity experiments. The time spans are different among these 6 tests: Case 1 (surface-CONTRAIL) and Case 2 (surface-Only) run for the period 2006-2010 (2000-2005 servers as a spin-up period), while Cases 3 to 6 run for the period 2008-2010. To compare other alternative sensitivity estimates for the same period from 2008 to 2010, we calculated this three-year average of annual Asia CO_2 fluxes (2008-2010) from all the 6 tests to be −1.61, −1.15, −1.69, −1.80, −1.23 and −1.07 PgC yr^{-1}, respectively. The alternative in Asian CO_2 uptake ranges from −1.07 to −1.80 Pg C yr^{-1} across our sensitivity experiments, which complements the Gaussian error. Despite the small numbers of years included, this range suggests that the Asian terrestrial was a sizable sink, while a carbon source in previous studies implied by the 1-sigma Gaussian error of ±1.18 Pg C yr^{-1} on the estimated mean, is very unlikely. The largest sensitivity in inferred flux is to the change of land cover types (Case 6) and to the variations in prior terrestrial biosphere fluxes (Case 4). The inversion with updated Chinese fossil fuel emissions (Case 3) also shows large variations in the inverted CO_2 flux, while the sensitivity to the TM5 model resolution (Case 5) is generally modest.

3.2.5 Impacts of the CONTRAIL data on inverted Asian CO2 Flux

We examined the impacts of the CONTRAIL data on Asian flux estimation by comparing results from Case 1 (Surface-CONTRAIL) and Case 2 (Surface-Only)(Table 5 and Figure 8a). Note that the uncertainties shown in the Table 5 and Figure 8b are now the Gaussian uncertainties as we did not repeat all sensitivity experiments. As shown in Table 5, inclusion of the CONTRAIL data induces an averaged extra CO_2 sink of about −0.47 Pg C yr^{-1} to Case 1 (0.47 = 1.56 − 1.09), with most addition to the grass/shrub ecosystem (Figure 5). The spatial pattern of Asian

fluxes also changed considerably (see Figure 8a). For instance, a decrease in CO_2 uptake was found in the northern area of Boreal Eurasia together with an increase in the south of Boreal Eurasia, leading to almost identical total carbon sink strength in the Boreal Asia between with and without CONTRAIL data. Whereas the estimated flux distribution in the Tropical Asia showed a small spatial change and a large increase in regional sink size with CONTRAIL observations.

Table 5 and Figure 8b shows the reduction of Gaussian error between Case 1 and Case 2. The error reduction rate (ER) is calculated as a percentage:

$$ER = (\sigma_{Surface\text{-}Only} - \sigma_{Surface\text{-}CONTRAIL}) / \sigma_{Surface\text{-}Only} \times 100, \quad (2)$$

Where $\sigma_{Surface\text{-}Only}$ and $\sigma_{Surface\text{-}CONTRAIL}$ are Gaussian errors in Case 2 (Surface-Only) and Case 1 (Surface-CONTRAIL), respectively. By including the additional CONTRAIL data into the inversion system, the uncertainty of the posterior flux over Asia is significantly reduced (>10%), especially for the southeast of Boreal Eurasia, southeast of Temperate Eurasia and Tropical areas (up to 20-30%). A more pronounced reduction was found in Boreal Eurasia and Tropical Asia (reducing by 14% and 15%, respectively). This suggests that current surface CO_2 observations data alone do not sufficiently constrain these regional flux estimation (there are no observations sites in the Boreal Eurasia and only one in the Tropical Asia), and the additional CONTRAIL CO_2 observations impose an extra constraint that can help reduce uncertainty on inferred Asia CO_2 flux, especially for these two surface observation sparse regions. We also found the error reduction in Temperate Eurasia is relatively small (<10%), especially for the west of Temperate Eurasia (<1%) because of a relative abundance of surface CO_2 observations in this region.

4 Discussions and Conclusions

4.1 Impact of CONTRAIL

Our modeling experiments reveal that the extra aircraft observation data shift the inverted CO_2 flux estimates by imposing further constraints. This confirms the earlier

findings by Saeki, *et al.* (2003) and Maksyutov, *et al.* (2013) that the inverted fluxes were sensitive to observation data used. For Tropical Asia, inclusion of the CONTRAIL data notably reduced the uncertainties (about 15% reduction). Compared with an inversion study with the CONTRAIL data for the Tropical Asia region (Niwa et al., 2012) , the error reduction rate in land flux estimation in this study (15%) for the same region is smaller than that of Niwa, *et al.* (34%). This difference in uncertainty reduction likely results from the differences in revision system design between these two studies, of which vertical mixing represented in transport model, the CO_2 network used in system and covariance assigned to prior fluxes are typically most important. We furthermore note that the set of observation used in these studies was not identical, we for instance included one tropical surface site (BKT, see Table 1 and Figure 2a) to constrain the inferred flux estimation but Niwa, *et al.* (2012) did not.

Our results share other features with the Niwa *et al.* (2012) study, for instance the largest impact on the least data constrained regions. Reported by Niwa, *et al.* (2012), the inclusion of CONTRAIL measurements not only constrains the nearby fluxes, but also reduces inferred flux errors in the regions far from the CONTRAIL measurement locations. For instance, in Boreal Eurasia, where no surface site exists and which is far from the CONTRAIL data locations (after pre-processing of horizontal/vertical bins and filter operation of stratospheric, there is no CONTRAIL observation available over this region), uncertainty reductions are large (14% reduction in uncertainty). Similar results were also presented by Niwa, *et al.* (2012), with an 18% error reduction in Boreal Eurasia. These two studies consistently suggest that including the CONTRAIL measurements in inversion modeling systems will help to increase the NEE estimation accuracy over Boreal Eurasia.

The CONTRAIL contribution to Temperate Eurasia is generally modest, only having a 6% error reduction. This may due to that Temperate Eurasia has more surface observation sites than other regions in Asia. However, it is interesting that the difference in inverted NEE in this region between Surface-Only and Surface-CONTRAIL is large (−0.35 Pg C yr^{-1}), but inconsistent with Niwa *et al.*

(2012). One cause of this is likely the sensitivity of these inverse systems to vertical transport (Stephens et al., 2007), as also suggested by Niwa*, et al.*(2012). The uneven distribution of observations at the surface and free troposphere may also aggravate this discrepancy.

4.2 Comparison of the estimated Asian CO_2 Flux with other studies

Our estimated Asian terrestrial carbon sink is about −1.56 Pg C yr^{-1} for the period 2006-2010. Most parts of Asian were estimated to be CO_2 sinks, with the largest carbon sink (−1.02 Pg C yr^{-1}) in Boreal Eurasia, a second large CO_2 sink (−0.68 Pg C yr^{-1}) in Temperate Eurasia, while a small source (+0.15 Pg C yr^{-1}) in Tropical Asia. This spatial distributions of estimated terrestrial CO_2 fluxes are overall comparable to the results for the period of 2000 to 2009 by Saeki *et al*. (2013), derived from an inversion approach focusing on Siberia with additional Siberian aircraft and tower CO_2 measurements, especially in the high latitude areas.

Comparisons of our inverted CO_2 flux with previous studies are summarized in Table 6. In Boreal Eurasia, our inferred land flux (−1.02 Pg C yr^{-1}) is higher than Gurney *et al.* (2003) (−0.59 Pg C yr^{-1} during 1992-1996), but close to Maki *et al.* (2010) (−1.46 Pg C yr^{-1} during 2001-2007), CTE2013 (−0.93 Pg C yr^{-1}) and CT2011_oi (−1.00 Pg C yr^{-1}, downloaded from http://carbontracker.noaa.gov). In Temperate Eurasia, our inverted flux is −0.68 Pg C yr^{-1}, which is well consistent with Gurney *et al.* (2003) (−0.60 Pg C yr^{-1}), but higher than CTE2013 (−0.33 Pg C yr^{-1}) and CT2011_oi (−0.41 Pg C yr^{-1}) even though we used a similar inversion framework. One reason of this discrepancy is likely that different zoomed regions were configured in the inversion system. Another main factor is likely the inclusion of CONTRAIL largely impacts on our Temperate Eurasia's carbon estimates. In Tropical Asia, our estimate is +0.15 Pg C yr^{-1}, which is in the range of Niwa *et al.*(2012) (+0.45 Pg C yr^{-1}) and Patra *et al.*(2013) (−0.104 Pg C yr^{-1}), both including aircraft CO_2 measurements in their inversion modeling, and very close to the CTE2013 (+0.22 Pg C yr^{-1}) and CT2011_oi (+0.14 Pg C yr^{-1}). The estimated total Asian terrestrial carbon sink is −1.56 Pg C yr^{-1}, which is close to the CTE2013 (−1.05 Pg C yr^{-1}) and CT2011_oi (−1.27 Pg C yr^{-1}). The IAVs comparison between the results from

this study and from CTE2013/CT2011_oi is also presented in Table 7 (different from IAV in Section 3.2.2, these results include biomass burning emissions). The IAVs are different between approaches. In 2007, there was a moderate Asian CO_2 sink in CTE2013 and CT2011_oi, while the results from this study show Asian was the highest carbon uptake during this study period, corresponding to strong CO_2 sinks in Eurasia Temperate and Eurasia Boreal areas. In 2008, Asian was the strongest terrestrial CO_2 sink from CTE2013 and CT2011_oi, while from our estimates that the sink in 2008 in Asian was weaker than that in 2007. In Asian, 2009 was a lower-than-average land sink in CTE2013 and a normal carbon sink in CT2011_oi, while from our results 2009 was the second strongest carbon uptake year. This discrepancy likely stems from the additions of Asia sites and CONTRAIL data in this study. Compared to previous findings, our updated estimation with these additional data seems to support a larger Asian carbon sink over the past decade.

The spatial patterns of NEE in Asia are complex because of large land surface heterogeneity, such as land cover, vegetation growth, soil types, etc. In addition, climate change and land use change and human activities impose on seasonal and interannual changes in NEE. All these factors make that to accurately estimate NEE over Asia area is a big challenge. We believe this study is therefore useful to improve our understanding of the Asia regional terrestrial carbon cycle processes even though our estimation still exhibit considerable uncertainties and biases in the inverted fluxes due to data availability and limited methodology. By these comparisons, we can also conclude that our inferred Asia land surface CO_2 fluxes support a view that both large boreal and mid-latitude carbon sinks in Asian are balanced partly by a small tropical source. This would support the earlier suggestion that the Asia region is of key interest to better understand the global terrestrial carbon budget in the context of climate change.

The majority of the CO_2 sink was found in the areas dominated by forests, crops and grass/shrubs. Asian forests were estimated to be a large sink (-0.77 Pg C yr^{-1}) during 2006-2010, the sink size is slightly larger than the bottom-up derived results of Pan, *et*

al. (2011)(−0.62 Pg C yr^{-1}) for the period 1990-2007. One cause of this discrepancy is likely due to that our estimate is presented at a coarse resolution (a 1°×1° grid may contain other biomes with low carbon uptake than forests). Another reason may be that about half of the Temperate Eurasia was not included in the statistical analysis by Pan et al. (2011). Note that the carbon accumulation in wood products is not considered in our estimates and needs further analysis in future studies.

The croplands in Asia were identified to be an average sink of −0.20 Pg C yr^{-1} during 2006-2010. The uptake in croplands is likely associated with agricultural technique and cropping management. Different from other natural ecosystems, crop ecosystems are usually under intensive farming cultivation, with regular fertilizing and irrigation of the crops according to plants growing properties. These cultivation practice increases the crop production, and in return lead to high residues and root to the soil, which largely increase the carbon sink in cropland (Chen et al., 2013). However, the accumulation of crop carbon in most crop ecosystems is relatively low, in which agricultural areas are even considered no contribution to a long-term net sink (Fang et al., 2007; Piao et al., 2009; Tian et al., 2011). This is because the carbon accumulation in the crop biomass is harvested at least once per year and released back as CO_2 to the atmosphere. We should note that our estimate in the crop sink is different from the results of "crop no contribution " (Piao et al., 2009). Our atmospheric inversion system can well capture the crop's strong CO_2 uptake during growing season, but the atmosphere locally does not reflect the emission of the harvested crops, which normally has been transported laterally and is consumed elsewhere. This harvested product is likely released from a region with high population density and hard to detect against high fossil fuel emissions, whereas the estimated crop flux remains a large net CO_2 uptake over the period considered even though the crop flux into the soil is relatively small. Thus the croplands' sink in this study might be overestimated due to the absence of harvesting in our modeling system. This issue was also raised by Peters *et al*. (2007; 2010).

Grassland/Shrub ecosystems also play an important role in the global carbon cycle,

accounting for about 20% of total terrestrial production and could be a potential carbon sink in future (Scurlock and Hall, 1998). The grass/shrub lands in Asia absorb CO_2 of −0.44 Pg C yr^{-1}, accounting for about 25% of the total Asian terrestrial CO_2 sink, which is close to the averaged global grassland sink percentage of 20%. Compared to the bottom-up results that net ecosystem productivity was 10.18 g C m^{-2} yr^{-1} by Yu*, et al.* (2013), our estimate of 34.32 g C m^{-2} yr^{-1} is much higher. This might due to that the areas in this study include shrubs whereas other studies only considering grass lands.

Acknowledgements

We wish to thank the Dr. Y. Niwa of Geochemical Research Department, Meteorological Research Institute, Tsukuba, Japan for providing many important comparable results and useful comments on this study. We kindly acknowledge all atmospheric data providers to the ObsPack version 1.0.2, and those that contribute their data to WDCGG. We are grateful to Michel Ramonet of French RAMCES (Réseau Atmosphérique de Mesure des Composés à Effet de Serre), Angel J. Gomez-Pelaez of Izaña Atmospheric Research Center (IARC), Meteorological State Agency of Spain (AEMET), Spain, Britt Stephens of NCAR, Laszlo Haszpra of Hungarian Meteorological Service and Samuel Hammer of University of Heidelberg, Institut fuer Umweltphysik for CO_2 time series used in this assimilation system. This research is supported by the Strategic Priority Research Program “Climate Change: Carbon Budget and Related Issues" of the Chinese Academy of Sciences (Grant # XDA05040403)，the National High Technology Research and Development Program of China (Grant no. 2013AA122002)，the research grant (41271116) funded by the National Science Foundation of China, a Research Plan of LREIS (O88RA900KA), CAS, a research grant (2012ZD010) of Key Project for the Strategic Science Plan in IGSNRR, CAS, and “One Hundred Talents” program funded by the Chinese Academy of Sciences. Wouter Peters was supported by an NWO VIDI Grant (864.08.012) and the Chinese-Dutch collaboration was funded by the China Exchange Program project (12CDP006). I. van der Laan-Luijkx has received funding from the European Union's Seventh Framework Programme (FP7/2007-2013) under grant agreement n° 283080, project GEOCARBON.

References

Baker, D., Law, R., Gurney, K., Rayner, P., Peylin, P., Denning, A., Bousquet, P., Bruhwiler, L., Chen, Y. H., and Ciais, P.: TransCom 3 inversion intercomparison: Impact of transport model errors on the interannual variability of regional CO2 fluxes, 1988–2003, Global Biogeochem Cy, 20, GB1002, 2006.

Boden, T., Marland, G., and Andres, R.: Global, regional, and national fossil-fuel CO2 emissions, Carbon Dioxide Information Analysis Center, Oak Ridge National Laboratory, US Department of Energy, Oak Ridge, Tenn., USA doi 10.3334/CDIAC/00001_V2011, 10, 2011.

Broquet, G., Chevallier, F., Bréon, F. M., Kadygrov, N., Alemanno, M., Apadula, F., Hammer, S., Haszpra, L., Meinhardt, F., Morguí, J. A., Necki, J., Piacentino, S., Ramonet, M., Schmidt, M., Thompson, R. L., Vermeulen, A. T., Yver, C., and Ciais, P.: Regional inversion of CO2 ecosystem fluxes from atmospheric measurements: reliability of the uncertainty estimates, Atmos. Chem. Phys., 13, 9039-9056, 2013.

Cao, M., PRINCE, S. D., Li, K., TAO, B., SMALL, J., and Shao, X.: Response of terrestrial carbon uptake to climate interannual variability in China, Global Change Biol, 9, 536-546, 2003.

Chen, B., Chen, J. M., and Ju, W.: Remote sensing-based ecosystem-atmosphere simulation scheme (EASS)--Model formulation and test with multiple-year data, Ecol Model, 209, 277-300, 2007.

Chen, B., Coops, N. C., Fu, D., Margolis, H. A., Amiro, B. D., Black, T. A., Arain, M. A., Barr, A. G., Bourque, C. P. A., and Flanagan, L. B.: Characterizing spatial representativeness of flux tower eddy-covariance measurements across the Canadian Carbon Program Network using remote sensing and footprint analysis, Remote Sens Environ, 124, 742-755, 2012.

Chen, Z., Yu, G., Ge, J., Sun, X., Hirano, T., Saigusa, N., Wang, Q., Zhu, X., Zhang, Y., and Zhang, J.: Temperature and precipitation control of the spatial variation of terrestrial ecosystem carbon exchange in the Asian region, Agr Forest Meteorol, 2013.

Chevallier, F. and O'Dell, C. W.: Error statistics of Bayesian CO2 flux inversion schemes as seen from GOSAT, Geophys Res Lett, 2013.

Clark, D. A., Brown, S., Kicklighter, D. W., Chambers, J. Q., Thomlinson, J. R., and Ni, J.: Measuring net primary production in forests: concepts and field methods, Ecol Appl, 11, 356-370, 2001.

Commission, E.: Joint Research Centre (JRC)/Netherlands Environmental Assessment Agency (PBL): Emission Database for Global Atmospheric Research (EDGAR), release version 4.0. 2009.

Deng, F., Chen, J. M., Ishizawa, M., YUEN, C. W. A. I., Mo, G., Higuchi, K., Chan, D., and Maksyutov, S.: Global monthly CO2 flux inversion with a focus over North America, Tellus B, 59, 179-190, 2007.

Fan, Z. M., Li, J., and Yue, T. X.: Changes of Climate-Vegetation Ecosystem in Loess Plateau of China, Procedia Environmental Sciences, 13, 715-720, 2012.

Fang, J., Chen, A., Peng, C., Zhao, S., and Ci, L.: Changes in forest biomass carbon storage in China between 1949 and 1998, Science, 292, 2320, 2001.

Fang, J., Guo, Z., Piao, S., and Chen, A.: Terrestrial vegetation carbon sinks in China, 1981–2000, Science in China Series D: Earth Sciences, 50, 1341-1350, 2007.

Francey, R. J., Trudinger, C. M., van der Schoot, M., Law, R. M., Krummel, P. B., Langenfelds, R. L., Steele, L. P., Allison, C. E., Stavert, A. R., and Andres, R. J.: Atmospheric verification of anthropogenic CO2 emission trends, Nature Climate Change, 2013.

Friedl, M. A., McIver, D. K., Hodges, J. C., Zhang, X., Muchoney, D., Strahler, A. H., Woodcock, C. E., Gopal, S., Schneider, A., and Cooper, A.: Global land cover mapping from MODIS: algorithms and early results, Remote Sens Environ, 83, 287-302, 2002.

Giglio, L., Werf, G., Randerson, J., Collatz, G., and Kasibhatla, P.: Global estimation of burned area using MODIS active fire observations, Atmos Chem Phys, 6, 957-974, 2006.

Gurney, K. R., Baker, D., Rayner, P., and Denning, S.: Interannual variations in continental-scale net carbon exchange and sensitivity to observing networks estimated from atmospheric CO2 inversions for the period 1980 to 2005, Global Biogeochem. Cycles, 22, 3025, 2008.

Gurney, K. R., Law, R. M., Denning, A. S., Rayner, P. J., Baker, D., Bousquet, P., Bruhwiler, L., Chen, Y. H., Ciais, P., and Fan, S.: Towards robust regional estimates of CO2 sources and sinks using atmospheric transport models, Nature, 415, 626-630, 2002.

Gurney, K. R., Law, R. M., Denning, A. S., Rayner, P. J., Baker, D., Bousquet, P., Bruhwiler, L., CHEN, Y. H., Ciais, P., and Fan, S.: TransCom 3 CO2 inversion intercomparison: 1. Annual mean control results and sensitivity to transport and prior flux information, Tellus B, 55, 555-579, 2003.

Gurney, K. R., Law, R. M., Denning, A. S., Rayner, P. J., Pak, B. C., Baker, D., Bousquet, P., Bruhwiler, L., Chen, Y. H., and Ciais, P.: Transcom 3 inversion intercomparison: Model mean results for the estimation of seasonal carbon sources and sinks, Global Biogeochem. Cycles, 18, 2004.

Hayes, D. J., McGuire, A. D., Kicklighter, D. W., Gurney, K. R., Burnside, T., and Melillo, J. M.: Is the northern high-latitude land-based CO2 sink weakening?, Global Biogeochem Cy, 25, 2011.

Houghton, R.: Balancing the global carbon budget, Annu. Rev. Earth Planet. Sci., 35, 313-347, 2007.

Huber, M. and Knutti, R.: Anthropogenic and natural warming inferred from changes in Earth's energy balance, Nat Geosci, 2011.

Ichii, K., Kondo, M., Lee, Y.-H., Wang, S.-Q., Kim, J., Ueyama, M., Lim, H.-J., Shi, H., Suzuki, T., and Ito, A.: Site-level model–data synthesis of terrestrial carbon fluxes in the CarboEastAsia eddy-covariance observation network: toward future modeling efforts, Journal of Forest Research, 18, 13-20, 2013.

Ito, A.: The regional carbon budget of East Asia simulated with a terrestrial ecosystem model and validated using AsiaFlux data, Agr Forest Meteorol, 148, 738-747, 2008.

Jacobson, A. R., Mikaloff Fletcher, S. E., Gruber, N., Sarmiento, J. L., and Gloor, M.: A joint atmosphere-ocean inversion for surface fluxes of carbon dioxide: 1. methods and global-scale fluxes, Global Biogeochem Cy, 21, 2007.

Jiang, F., Wang, H. W., Chen, J. M., Zhou, L. X., Ju, W. M., Ding, A. J., Liu, L. X., and Peters, W.: Nested atmospheric inversion for the terrestrial carbon sources and sinks in China, Biogeosciences, 10, 5311-5324, 2013.

Krol, M., Houweling, S., Bregman, B., Van den Broek, M., Segers, A., Van Velthoven, P., Peters, W., Dentener, F., and Bergamaschi, P.: The two-way nested global chemistry-transport zoom model TM5: algorithm and applications, Atmos Chem Phys, 5, 417-432, 2005.

Le Quéré, C., Raupach, M. R., Canadell, J. G., and Marland, G.: Trends in the sources and sinks of carbon dioxide, Nat Geosci, 2, 831-836, 2009.

Le Quere, C., Raupach, M. R., Canadell, J. G., Marland, G., and et al.: Trends in the sources and sinks of carbon dioxide, Nature Geosci, 2, 831-836, 2009.

Machida, T., Matsueda, H., Sawa, Y., Nakagawa, Y., Hirotani, K., Kondo, N., Goto, K., Nakazawa, T., Ishikawa, K., and Ogawa, T.: Worldwide measurements of atmospheric CO2 and other trace gas species using commercial airlines, J Atmos Ocean Tech, 25, 1744-1754, 2008.

Machida, T., Tohjima, Y., Katsumata, K., and Mukai, H.: A new CO2 calibration scale based on gravimetric one-step dilution cylinders in National Institute for Environmental Studies-NIES 09 CO2 scale, World Meteorol. Organ., Geneva, Switzerland, 114-119, 2011.

Maki, T., Ikegami, M., Fujita, T., Hirahara, T., Yamada, K., Mori, K., Takeuchi, A., Tsutsumi, Y., Suda, K., and Conway, T.: New technique to analyse global distributions of CO2 concentrations and fluxes from non-processed observational data, Tellus B, 62, 797-809, 2010.

Maksyutov, S., Machida, T., Mukai, H., Patra, P. K., Nakazawa, T., and Inoue, G.: Effect of recent observations on Asian CO2 flux estimates by transport model inversions, Tellus B, 55, 522-529, 2003.

Marland, G., Boden, T. A., Andres, R. J., Brenkert, A., and Johnston, C.: Global, regional, and national fossil fuel CO2 emissions, Trends: A compendium of data on global change, 34-43, 2003.

Masarie, K., Pétron, G., Andrews, A., Bruhwiler, L., Conway, T., Jacobson, A., Miller, J., Tans, P., Worthy, D., and Peters, W.: Impact of CO2 measurement bias on CarbonTracker surface flux estimates, Journal of Geophysical Research, 116, D17305, 2011.

Masarie, K. A. and Tans, P. P.: Extension and integration of atmospheric carbon dioxide data into a globally consistent measurement record, Journal of Geophysical Research: Atmospheres (1984–2012), 100, 11593-11610, 1995.

Matsueda, H., Machida, T., Sawa, Y., Nakagawa, Y., Hirotani, K., Ikeda, H., Kondo, N., and Goto, K.: Evaluation of atmospheric CO sub (2) measurements from new flask air sampling of JAL airliner observations, Papers in Meteorology and Geophysics, 59, 1-17, 2008.

Mizoguchi, Y., Miyata, A., Ohtani, Y., Hirata, R., and Yuta, S.: A review of tower flux observation sites in Asia, Journal of Forest Research, 14, 1-9, 2009.

Mohammat, A., Wang, X., Xu, X., Peng, L., Yang, Y., Zhang, X., Myneni, R. B., and Piao, S.: Drought and spring cooling induced recent decrease in vegetation growth in Inner Asia, Agr Forest Meteorol, 2012.

NationalClimateCenter: 2010 China Climate Bulletin, China Meteorological Press, 1, 34, 2011.

Niwa, Y., Machida, T., Sawa, Y., Matsueda, H., Schuck, T. J., Brenninkmeijer, C. A. M., Imasu, R., and Satoh, M.: Imposing strong constraints on tropical terrestrial CO2 fluxes using passenger aircraft based measurements, Journal of Geophysical Research: Atmospheres, 117, D11303, 2012.

Niwa, Y., Patra, P., Sawa, Y., Machida, T., Matsueda, H., Belikov, D., Maki, T., Ikegami, M., Imasu, R., and Maksyutov, S.: Three-dimensional variations of atmospheric CO2: Aircraft measurements and multi-transport model simulations, Atmos. Chem. Phys, 11, 13359-13375, 2011.

Oikawa, T. and Ito, A.: Modeling carbon dynamics of terrestrial ecosystems in monsoon Asia, Present and future modeling global environmental change: toward integrated modeling. TERRAPUB, Tokyo, 207-219, 2001.

Olivier, J. and Berdowski, J.: Global emission sources and sinks, 2001.

Olson, J. S., Watts, J. A., and Allison, L. J.: Major World Ecosystem Complexes Ranked by Carbon in Live Vegetation: A Database, NDP-017, Oak Ridge Lab., Oak Ridge, Tenn, 1985.

Pan, Y., Birdsey, R. A., Fang, J., Houghton, R., Kauppi, P. E., Kurz, W. A., Phillips, O. L., Shvidenko, A., Lewis, S. L., Canadell, J. G., Ciais, P., Jackson, R. B., Pacala, S. W., McGuire, A. D., Piao, S., Rautiainen, A., Sitch, S., and Hayes, D.: A Large and Persistent Carbon Sink in the World's Forests, Science, 333, 988-993, 2011.

Patra, P., Canadell, J., Houghton, R., Piao, S., Oh, N.-H., Ciais, P., Manjunath, K., Chhabra, A., Wang, T., and Bhattacharya, T.: The carbon budget of South Asia, Biogeosciences, 10, 513-527, 2013.

Patra, P., Niwa, Y., Schuck, T., Brenninkmeijer, C., Machida, T., Matsueda, H., and Sawa, Y.: Carbon balance of South Asia constrained by passenger aircraft CO2 measurements, Atmos. Chem. Phys, 11, 4163-4175, 2011.

Patra, P. K., Canadell, J. G., and Lal, S.: The rapidly changing greenhouse gas budget of Asia, Eos,

Transactions American Geophysical Union, 93, 237-237, 2012.

Peters, G. P., Marland, G., Le Quéré, C., Boden, T., Canadell, J. G., and Raupach, M. R.: Rapid growth in CO2 emissions after the 2008-2009 global financial crisis, Nature Climate Change, 2, 2-4, 2011.

Peters, W., Jacobson, A. R., Sweeney, C., Andrews, A. E., Conway, T. J., Masarie, K., Miller, J. B., Bruhwiler, L. M. P., Petron, G., and Hirsch, A. I.: An atmospheric perspective on North American carbon dioxide exchange: CarbonTracker, Proceedings of the National Academy of Sciences, 104, 18925, 2007.

Peters, W., Krol, M., Van der Werf, G., Houweling, S., Jones, C., Hughes, J., Schaefer, K., Masarie, K., Jacobson, A., and Miller, J.: Seven years of recent European net terrestrial carbon dioxide exchange constrained by atmospheric observations, Global Change Biol, 16, 1317-1337, 2010.

Peylin, P., R. Law, K. Gurney, F. Chevallier, A. Jacobson, T. Maki, Y. Niwa, P. Patra, W. Peters, and P. Rayner (2013), Global atmospheric carbon budget: results from an ensemble of atmospheric CO 2 inversions, Biogeosciences, 10(3), 5301-5360, doi:10.5194/bg-10-6699-2013.

Peylin, P., Rayner, P., Bousquet, P., Carouge, C., Hourdin, F., Heinrich, P., and Ciais, P.: Daily CO 2 flux estimates over Europe from continuous atmospheric measurements: 1, inverse methodology, Atmos Chem Phys, 5, 3173-3186, 2005.

Piao, S., Fang, J., Ciais, P., Peylin, P., Huang, Y., Sitch, S., and Wang, T.: The carbon balance of terrestrial ecosystems in China, Nature, 458, 1009-1013, 2009.

Piao, S. L., Ciais, P., Lomas, M., Beer, C., Liu, H. Y., Fang, J. Y., Friedlingstein, P., Huang, Y., Muraoka, H., Son, Y. H., and Woodward, I.: Contribution of climate change and rising CO(2) to terrestrial carbon balance in East Asia: A multi-model analysis, Global Planet Change, 75, 133-142, 2011.

Piao, S. L., Ito, A., Li, S. G., Huang, Y., Ciais, P., Wang, X. H., Peng, S. S., Nan, H. J., Zhao, C., Ahlström, A., Andres, R. J., Chevallier, F., Fang, J. Y., Hartmann, J., Huntingford, C., Jeong, S., Levis, S., Levy, P. E., Li, J. S., Lomas, M. R., Mao, J. F., Mayorga, E., Mohammat, A., Muraoka, H., Peng, C. H., Peylin, P., Poulter, B., Shen, Z. H., Shi, X., Sitch, S., Tao, S., Tian, H. Q., Wu, X. P., Xu, M., Yu, G. R., Viovy, N., Zaehle, S., Zeng, N., and Zhu, B.: The carbon budget of terrestrial ecosystems in East Asia over the last two decades, Biogeosciences, 9, 3571-3586, 2012.

Randall, D. A., Dazlich, D. A., Zhang, C., Denning, A. S., Sellers, P. J., Tucker, C. J., Bounoua, L., Los, S. O., Justice, C. O., and Fung, I.: A revised land surface parameterization (SiB2) for GCMs .3. The greening of the Colorado State University general circulation model, J Climate, 9, 738-763, 1996.

Randerson, J. T., Thompson, M. V., Conway, T. J., Fung, I. Y., and Field, C. B.: The contribution of terrestrial sources and sinks to trends in the seasonal cycle of atmospheric carbon dioxide, Global Biogeochem Cy, 11, 535-560, 1997.

Raupach, M. R., Marland, G., Ciais, P., Le Quéré, C., Canadell, J. G., Klepper, G., and Field, C. B.: Global and regional drivers of accelerating CO2 emissions, Proceedings of the National Academy of Sciences, 104, 10288-10293, 2007.

Richardson, A. D., Hollinger, D. Y., Dail, D. B., Lee, J. T., Munger, J. W., and O'keefe, J.: Influence of spring phenology on seasonal and annual carbon balance in two contrasting New England forests, Tree Physiol, 29, 321-331, 2009.

Rivier, L., Peylin, P., Ciais, P., Gloor, M., Rödenbeck, C., Geels, C., Karstens, U., Bousquet, P., Brandt, J., and Heimann, M.: European CO2 fluxes from atmospheric inversions using regional and global transport models. In: Greenhouse Gas Inventories, Springer, 2011.

Rivier, L., Peylin, P., Ciais, P., Gloor, M., Rödenbeck, C., Geels, C., Karstens, U., Bousquet, P., Brandt, J., and Heimann, M.: European CO2 fluxes from atmospheric inversions using regional and global

transport models, Climatic Change, 103, 93-115, 2010.

Saeki, T., Maksyutov, S., Sasakawa, M., Machida, T., Arshinov, M., Tans, P., Conway, T., Saito, M., Valsala, V., and Oda, T.: Carbon flux estimation for Siberia by inverse modeling constrained by aircraft and tower CO2 measurements, Journal of Geophysical Research: Atmospheres, 1-23, 2013.

Sawa, Y., Machida, T., and Matsueda, H.: Seasonal variations of CO2 near the tropopause observed by commercial aircraft, Journal of Geophysical Research, 113, D23301, 2008.

Scurlock, J. and Hall, D.: The global carbon sink: a grassland perspective, Global Change Biol, 4, 229-233, 1998.

Sellers, P., Mintz, Y., Sud, Y., and Dalcher, A.: A simple biosphere model (SiB) for use within general circulation models, J Atmos Sci, 43, 505-531, 1986.

Sellers, P., Randall, D., Collatz, G., Berry, J., Field, C., Dazlich, D., Zhang, C., Collelo, G., and Bounoua, L.: A revised land surface parameterization (SiB2) for atmospheric GCMs. Part I: Model formulation, J Climate, 9, 676-705, 1996.

Stephens, B. B., Gurney, K. R., Tans, P. P., Sweeney, C., Peters, W., Bruhwiler, L., Ciais, P., Ramonet, M., Bousquet, P., and Nakazawa, T.: Weak northern and strong tropical land carbon uptake from vertical profiles of atmospheric CO2, Science, 316, 1732-1735, 2007.

Takahashi, T., Wanninkhof, R., Feely, R., Weiss, R., Chipman, D., Bates, N., Olafsson, J., Sabine, C., and Sutherland, S.: Net sea-air CO2 flux over the global oceans: An improved estimate based on the sea-air pCO2 difference, 1999.

Thoning, K. W., Tans, P. P., and Komhyr, W. D.: Atmospheric carbon dioxide at Mauna Loa Observatory: 2. Analysis of the NOAA GMCC data, 1974–1985, Journal of Geophysical Research: Atmospheres (1984–2012), 94, 8549-8565, 1989.

Tian, H., Melillo, J., Lu, C., Kicklighter, D., Liu, M., Ren, W., Xu, X., Chen, G., Zhang, C., and Pan, S.: China's terrestrial carbon balance: Contributions from multiple global change factors, Global Biogeochem Cy, 25, 2011.

van der Werf, G. R., J. T. Randerson, L. Giglio, G. J. Collatz, P. S. Kasibhatla, and A. F. Arellano Jr (2006b), Interannual variability in global biomass burning emissions from 1997 to 2004, Atmos. Chem. Phys., 6(11), 3423-3441, doi:10.5194/acp-6-3423-2006.

Wai, K. M., Lin, N. H., Wang, S. H., and Dokiya, Y.: Rainwater chemistry at a high-altitude station, Mt. Lulin, Taiwan: Comparison with a background station, Mt. Fuji, Journal of Geophysical Research: Atmospheres (1984–2012), 113, 2008.

Walther, G.-R., Post, E., Convey, P., Menzel, A., Parmesan, C., Beebee, T. J., Fromentin, J.-M., Hoegh-Guldberg, O., and Bairlein, F.: Ecological responses to recent climate change, Nature, 416, 389-395, 2002.

Wang, H., Zhang, R., Liu, M., and Bi, J.: The carbon emissions of Chinese cities, Atmos Chem Phys, 12, 6197-6206, 2012.

Wang, X., Piao, S., Ciais, P., Li, J., Friedlingstein, P., Koven, C., and Chen, A.: Spring temperature change and its implication in the change of vegetation growth in North America from 1982 to 2006, Proceedings of the National Academy of Sciences, 108, 1240-1245, 2011.

Werf, G., Randerson, J. T., Giglio, L., Collatz, G. J., Kasibhatla, P. S., and Arellano Jr, A.: Interannual variability in global biomass burning emissions from 1997 to 2004, Atmos Chem Phys, 6, 3423-3441, 2006.

Yang, Z., Washenfelder, R., Keppel-Aleks, G., Krakauer, N., Randerson, J., Tans, P., Sweeney, C., and Wennberg, P.: New constraints on Northern Hemisphere growing season net flux, Geophys Res Lett, 34,

L12807, 2007.
Yu, G. R., Zhu, X. J., Fu, Y. L., He, H. L., Wang, Q. F., Wen, X. F., Li, X. R., Zhang, L. M., Zhang, L., and Su, W.: Spatial patterns and climate drivers of carbon fluxes in terrestrial ecosystems of China, Global Change Biol, 19, 798-810, 2013.

Tables and figure captions

Tables

Table 1 Summary of the 14 Asian surface CO_2 observation data assimilated between January 1, 2006 and December 31, 2010. The frequency of continuous data is one per day (when available), while discrete surface data point is generally once per week. MDM (model-data-mismatch) is a value assigned to a given site that is meant to quantify our expected ability to simulate observations and used to calculate the innovation X2 (Inn. X2) statistics. N denotes that the number is available in the CTDAS. Flagged observations mean a model-minus-observation difference that exceeds 3 times of the model-data-mismatch and were therefore excluded from assimilation. The bias is the average from posterior residuals (assimilated values – measured values), while the modeled bias is the average from prior residuals (modeled values – measured values)

Site	Name	Lat, Lon, Elev.	Lab	N(flagged)	MDM	Inn. X^2	Bias(modeled)
Discrete samples in Asia:							
1 WLG	Waliguan,China	36.29°N,100.90°E,3810m	CMA/ESRL	254(19)	1.5	0.83	-0.10(-0.14)
2 BKT	Bukit Kototabang,Indonesia	0.20°S,100.312°E,864m	ESRL	172(0)	7.5	0.73	5.53(5.51)
3 WIS	Sede Boker,Israel	31.13°N,34.88°E,400m	ESRL	239(1)	2.5	0.62	-0.10(-0.15)
4 KZD	Sary Taukum,Kazakhstan	44.45°N,77.57°E,412m	ESRL	167(6)	2.5	1.16	-0.08(0.50)

5 KZM	Plateau Assy,Kazakhstan	43.25°N ,77.88°E,2519m	ESRL	155(2)	2.5	0.96	0.50(0.63)
6 TAP	Tae-ahn Peninsula,Korea	36.73°N,126.13°E,20m	ESRL	181(3)	7.5	0.60	1.82(2.13)
7 UUM	Ulaan Uul,Mongolia	44.45°N,111.10°E,914m	ESRL	231(5)	2.5	1.17	0.10(0.28)
8 CRI	Cape Rama,India	15.08°N,73.83°E,60m	CSIRO	33(1)	3	1.40	-1.97(-2.11)
9 LLN	Lulin,Taiwan	23.47°N,120.87°E,2862m	ESRL	220(20)	7.5	0.99	2.62(2.65)
10 SDZ	Shangdianzi, China	40.39°N,117.07°E,287m	CMA/ESRL	60(15)	3	1.18	0.15(0.18)
continuous samples in Asia:							
11 MNM	Minamitorishima,Japan	24.29°N,153.98°E,8m	JMA	1624(0)	3	0.76	0.15(0.16)
12 RYO	Ryori,Japan	39.03°N,141.82°E,260m	JMA	1663(48)	3	0.90	0.46(0.69)
13 YON	Yonagunijima, Japan	24.47°N,123.02°E,30m	JMA	1684(3)	3	0.78	1.53(1.67)
14 GSN	Gosan, Republic of Korea	33.15°N,126.12°E,72m	NIER	1274(109)	3	1.99	-1.01(-0.82)

Table 2 Summary of the Asian CONTRAIL CO2 observation data assimilated between 2006 and 2010. MDM (model-data-mismatch) is a value assigned to a given site that is meant to quantify our expected ability to simulate observations and used to calculate the innovation X^2 (Inn. X^2) statistics. *N* denotes the number available in the CTDAS. Flagged observations mean a model-minus-observation difference that exceeds 3 times of the model-data-mismatch and are therefore excluded from assimilation. The MDM is the average of the posterior residuals (assimilated values – measured values), while the modeled bias is the average of prior residuals (modeled values – measured values).

Pressure Level	N(flagged)	MDM	Inn. X^2	Bias(modeled)
575-625 hPa	0	2.00	0.00	0.00
485-525 hPa	2907(5)	2.00	0.35	0.05(0.08)
375-425 hPa	3035(3)	2.00	0.34	-0.05(-0.07)
225-275 hPa	4525(4)	2.00	0.34	0.04(0.05)

Table 3 Results of the sensitivity experiments conducted in this study (Pg C yr^{-1})[a]

Inversion ID	Case 1	Case 2	Case 3	Case 4	Case 5	Case 6
Boreal Eurasia	-1.02	-0.96	-1.11	-1.25	-1.03	-0.92
Temperate Eurasia	-0.68	-0.33	-0.70	-0.63	-0.37	-0.36
Tropical Asia	0.15	0.19	0.12	0.08	0.17	0.20
Total Asia	-1.56	-1.09	-1.69	-1.80	-1.23	-1.07
NH land sink	-2.93	-2.64	-3.20	-3.20	-2.79	-2.70
Land	-2.43	-2.24	-3.07	-3.25	-2.65	-2.50
Ocean	-2.08	-2.16	-2.04	-2.05	-2.27	-2.18
Global	-4.50	-4.41	-5.12	-5.30	-4.92	-4.68

[a]The Case 1 (Surface-CONTRAIL) and Case 2 (Surface-Only) run for the period 2006-2010, while Case 3-6 run for the period 2008-2010; detailed discussion on global flux estimates can be found in SI Appendix B.

Table 4 Terrestrial biosphere fluxes considered in ecosystem types for 2006-2010 (Pg C yr^{-1})

	type	Asia	Boreal Eurasia	Temperate Eurasia	Tropical Asia	Asia	Boreal Eurasia	Temperate Eurasia	Tropical Asia
Forest	Conifer Forest	-0.64	-0.63	-0.02	0.00	-0.77	-0.71	-0.11	+0.04
	Broadleaf Forest	-0.04	-0.01	-0.01	-0.01				
	Mixed Forest	-0.14	-0.05	-0.07	-0.03				
	Fields/Woods/Savanna	-0.01	-0.01	0.00	0.00				
	Forest/Field	-0.02	-0.01	-0.01	0.00				
	Tropical Forest	+0.08	0.00	0.00	+0.08				
Grass/Shrub	Grass/Shrub	-0.43	-0.06	-0.36	-0.02	-0.44	-0.06	-0.36	-0.02
	Scrub/Woods	0.00	0.00	0.00	0.00				
	Shrub/Tree/Suc.	0.00	0.00	0.00	0.00				
crop	Crops	-0.20	-0.02	-0.17	-0.01	-0.20	-0.02	-0.17	-0.01

	Semitundra	-0.09	-0.05	-0.04	0.00				
	Northern Taiga	-0.17	-0.17	0.00	0.00				
	Wooded tundra	0.00	0.00	0.00	+0.06				
others	Mangrove	0.00	0.00	0.00	0.00	-0.15	-0.23	-0.04	+0.13
	Non-optimized	0.00	0.00	0.00	0.00				
	Water	0.07	0.00	0.00	+0.07				
	Wetland	+0.04	-0.01	0.00	0.00				
	Deserts	0.00	0.00	0.00	0.00				

Table 5 The prior/posterior land fluxes, biomass burning (fire) emissions, fossil fuel emissions and net land flux as well as the Gaussian error/their error reduction rates in Surface-Only and Surface-CONTRAIL inversion experiments during 2006-2010 (in Pg C yr^{-1})

	Prior Land	Fire	Fossil-fuel	Post. Land Flux		Post. Net Land Flux [a]		Gaussian error
Region	Flux	Emission	Emission	Surface-Only	Surface-CONTRAIL	Surface-Only	Surface-CONTRAIL	Error reduction (%)
Boreal Eurasia	-0.10±1.16	0.13	0.21	-1.09±1.05	-1.15±0.91	-0.96±1.05	-1.02±0.91	14
Temperate Eurasia	-0.15±0.93	0.03	3.31	-0.36±0.75	-0.70±0.70	-0.33±0.75	-0.68±0.70	6
tropical Asia	-0.10±0.35	0.32	0.63	-0.13±0.33	-0.17±0.28	0.20±0.33	0.15±0.28	15
Total Asia	-0.35±1.53	0.47	4.15	-1.56±1.34	-2.02±1.18	-1.09±1.34	-1.56±1.18	11

[a]Posterior Net Land Flux: including posterior land flux and fire emissions, but excluding fossil emissions.

Table 6 Comparison of the inverted Asia terrestrial ecosystem carbon fluxes (in Pg C yr^{-1}) from this study with previous studies

Reference	Period	Boreal Eurasia	Temperate Eurasia	Tropical Asia	Asia	Remarks
This study	2006-2010	-1.02±0.91	-0.68±0.70	+0.15±0.28	-1.56±1.18	Surface-CONTRAIL
[Gurney *et al.*,2003]	1992-1996	-0.59±0.52	-0.60±0.67	+0.67±0.70	-0.52±0.65	–
[Maki *et al.*,2010]	2001-2007	-1.46±0.41	0.96±0.59	-0.15±0.44	-0.65±0.49	CNTL experiments
CTE2013[a]	2006-2010	-0.93±1.15	−0.33±0.56	+0.22±0.20	-1.05±1.29	Focused on North America and Europe
CT2011_oi[b]	2006-2010	-1.00	–0.41	+0.14	–1.27	Focused on North America
[Niwa *et al.*,2012][c]	2006-2008	-	-	+0.45±0.19	-	GVCT

[a]CTE2013 : Carbon Tracker Europe in the pylin et al. (2013) for the period of 2006-2010

[b]CT2011_oi : downloaded from http://carbontracker.noaa.gov; without providing uncertainties

[c] GVCT : jointly using GLOBALVIEW and CONTRAIL CO_2 observation data to perform inversion

Table 7 Comparison of IAVs of the terrestrial ecosystem carbon fluxes in Asia during 2006-2010 from this study with previous studies. These fluxes (in Pg C yr^{-1}) include biomass burning emissions but exclude fossil fuel emissions

Reference	year	Asia	Boreal Eurasia	Eurasia temperate	tropical Asia
This study	2006	-1.16	-0.93	-0.60	0.37
	2007	-1.83	-1.17	-0.80	0.14
	2008	-1.71	-0.96	-0.66	-0.09
	2009	-1.80	-1.04	-0.88	0.12
	2010	-1.31	-1.01	-0.49	0.19
CTE2013	2006	-0.92	-0.93	-0.40	0.41
	2007	-1.14	-0.88	-0.44	0.18
	2008	-1.39	-1.07	-0.33	0.00
	2009	-0.87	-0.78	-0.34	0.25
	2010	-0.86	-1.02	-0.12	0.27
CT2011_oi	2006	-0.99	-0.78	-0.46	0.25
	2007	-1.25	-0.92	-0.46	0.13
	2008	-1.51	-1.13	-0.38	0.00
	2009	-1.40	-0.99	-0.51	0.10
	2010	-1.15	-1.16	-0.22	0.23

Figures

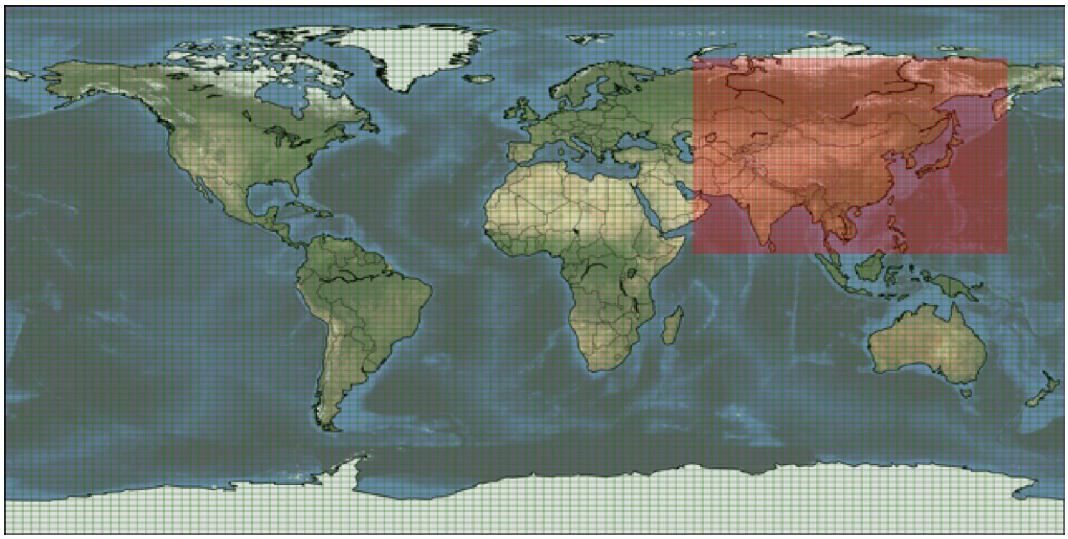

Figure 1 TM5 global grid (3×2) with zoom over Asia (1×1)

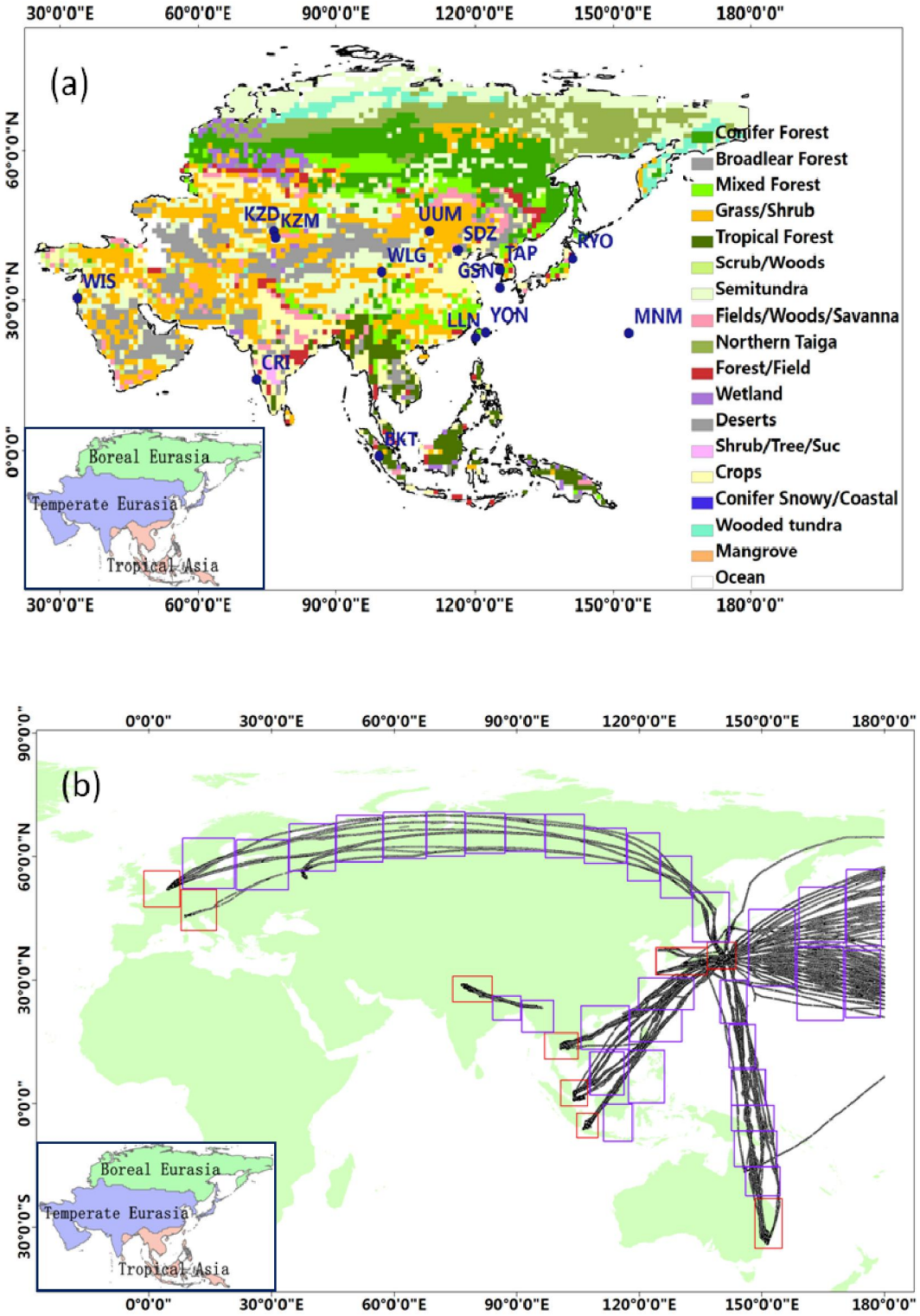

Figure 2 (a) Map of the Asian surface observation sites, along with the map of the ecoregion types from Olson, *et al.* (1985) with 19 land cover classes as used in this study. These observation data download from the NOAA-ESRL and WDCGG network in Figure 2a; (b) CONTRAIL CO_2 observations map, along with 42

horizontal regions. The red rectangles represent the 9 regions covering the ascending and descending data (included 4 vertical bins at 575-625, 475-525, 375-425, 225-275 hPa) over airports, and the blue rectangles indicate the other 33 regions covering the cruise data (included 1 bin at 225-275 hPa). Note that "Asia" refers to lands as far west as the Urals in this study and it is further divided into Boreal Eurasia, Temperate Eurasia and tropical Asia based on TransCom regions (Gurney et al., 2002; Gurney et al., 2003). These divided regions are presented in the small inset in the bottom left corner (same as thereafter)

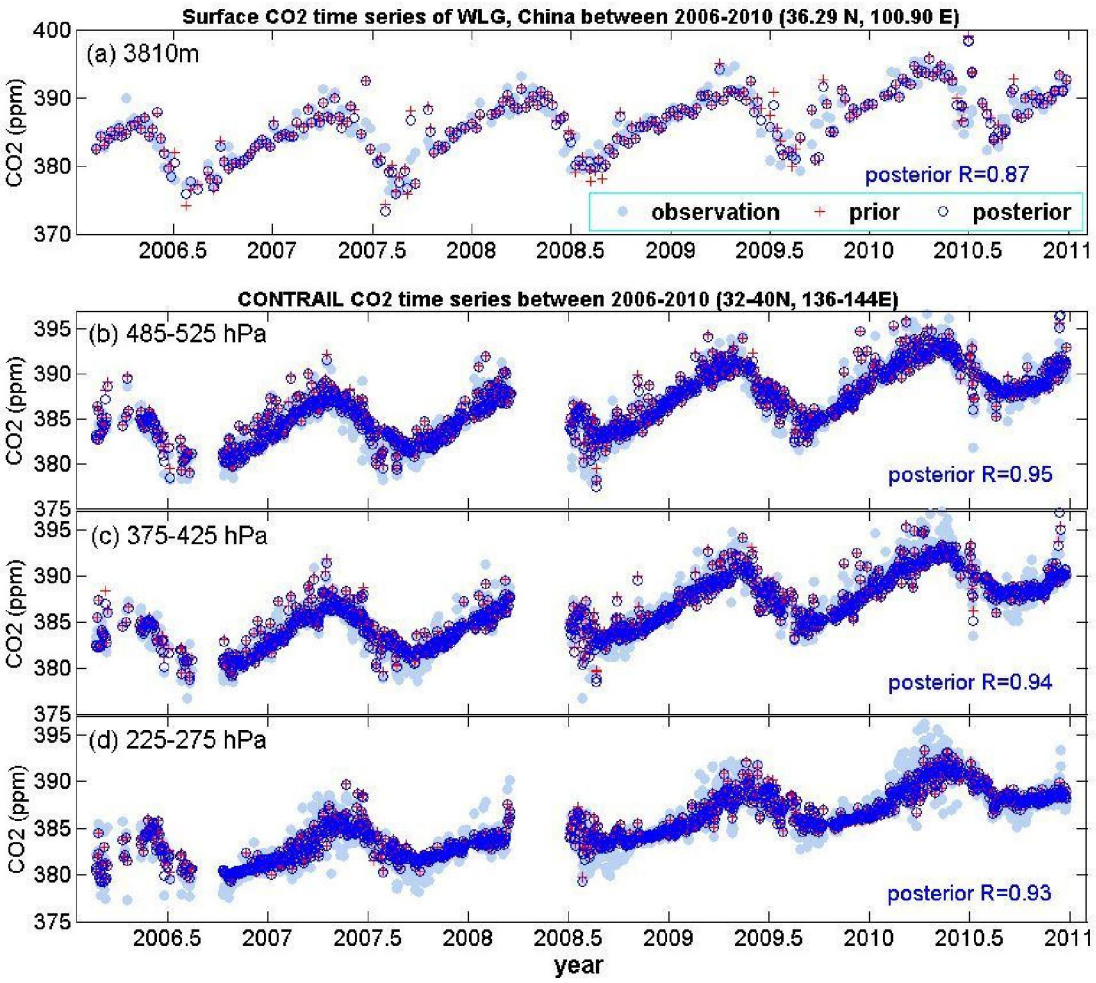

Figure 3 Comparison of modeled values with observed CO_2 concentrations from surface flask station (a) Mt. Waliguan (WLG), located in China; and from CONTRAIL data in the region covering 136-144°N, 32-40°E for three different vertical bins: (b) 485-525 hPa; (c) 375-425 hPa; (d) 225-275. Although 4 vertical bins (575–625, 475–525, 375–425, 225–275 hPa) of CONTRAIL measurements have been selected and added into the system, only 3 vertical bins observations have really been assimilated as sparse measurements associated to the 575–625 hPa in CONTRAIL data. Note that the prior CO_2 concentrations here are not really based on a-priori fluxes only, as they are a forecast started from the CO_2 mixing ratio field that contains all the already optimized fluxes (1,…, n-1) that occurred before the current cycle of the data assimilation system (n). So these prior mole fractions only contain five weeks (five weeks are the lag windows in our system) of recent un-optimized fluxes and constitute our 'first-guess' of atmospheric CO_2 for each site.

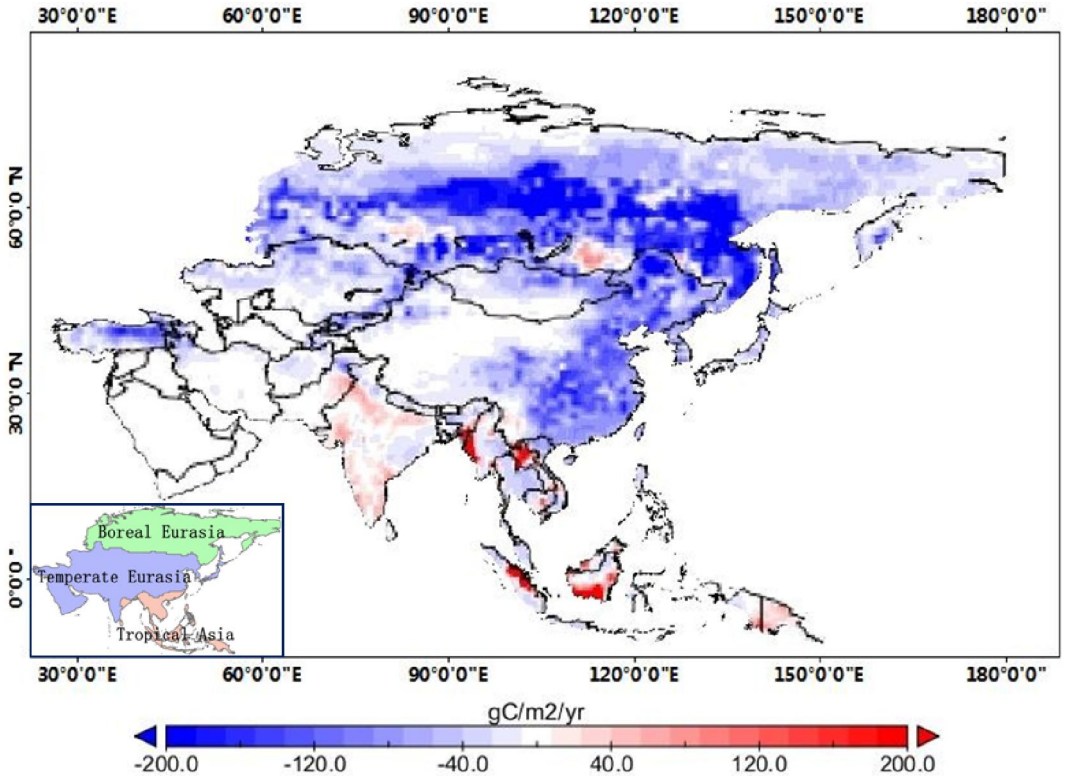

Figure 4 Mean terrestrial biosphere carbon flux estimated from our system over Asia during 2006-2010 at a 1×1 grid resolution. Blue colors (negative) denote net carbon uptake while red colors (positive) denote carbon release to the atmosphere. Note that the estimated flux map includes net terrestrial fluxes and biomass burning sources but excludes fossil fuel emissions.

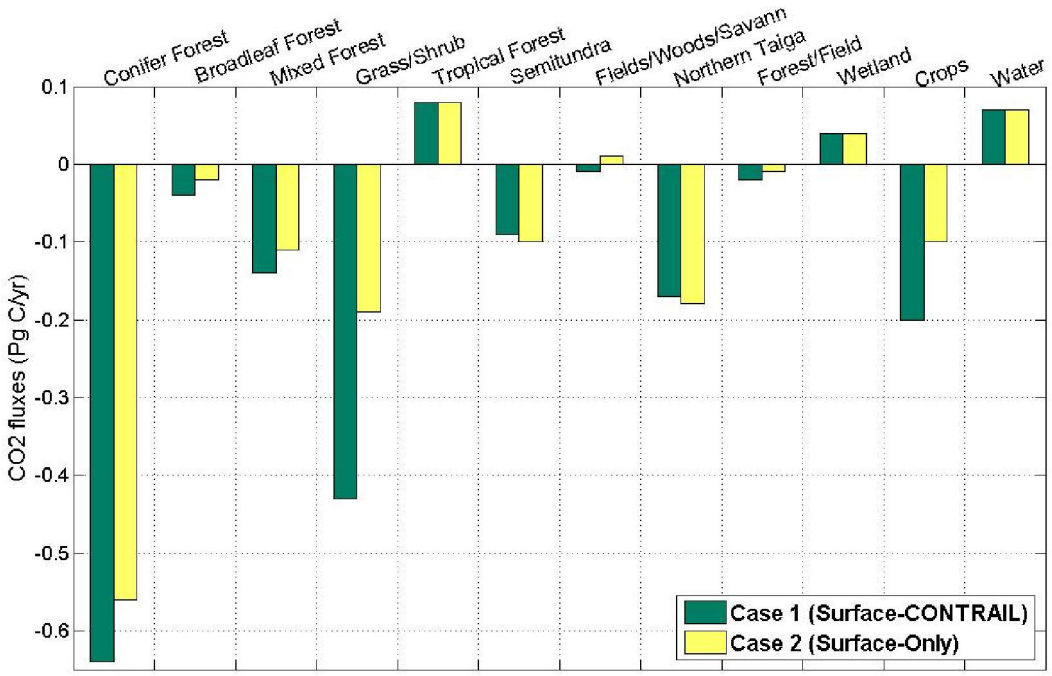

Figure 5 Fluxes per ecoregion in Asia averaged over the period 2006-2010 in Cases 1 and 2 (in Pg C yr^{-1}).

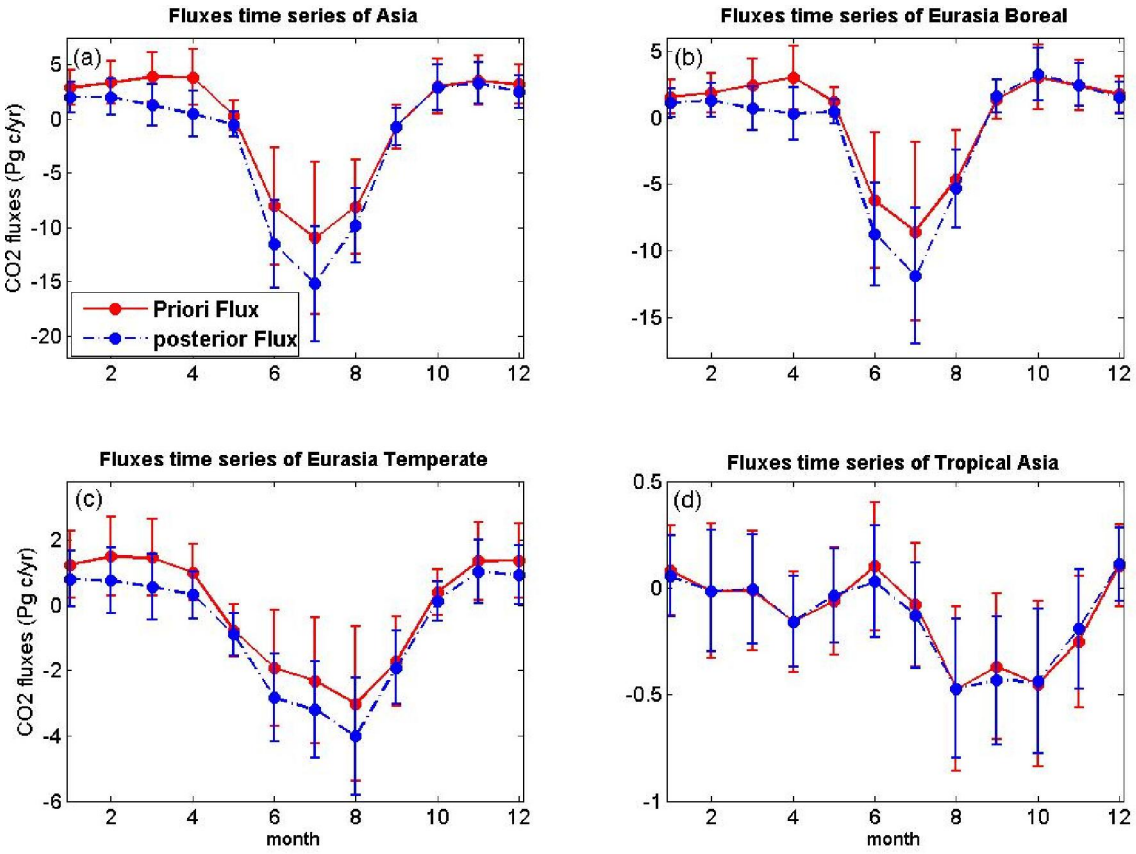

Figure 6 A priori and posteriori averaged fluxes (with uncertainties) over Asian regions during 2006-2010: (a) Asia; (b) Eurasia Boreal; (c) Eurasia Temperate; (d) Tropical Asia. This flux is biosphere carbon sink after removal of fossil and biomass burning fluxes.

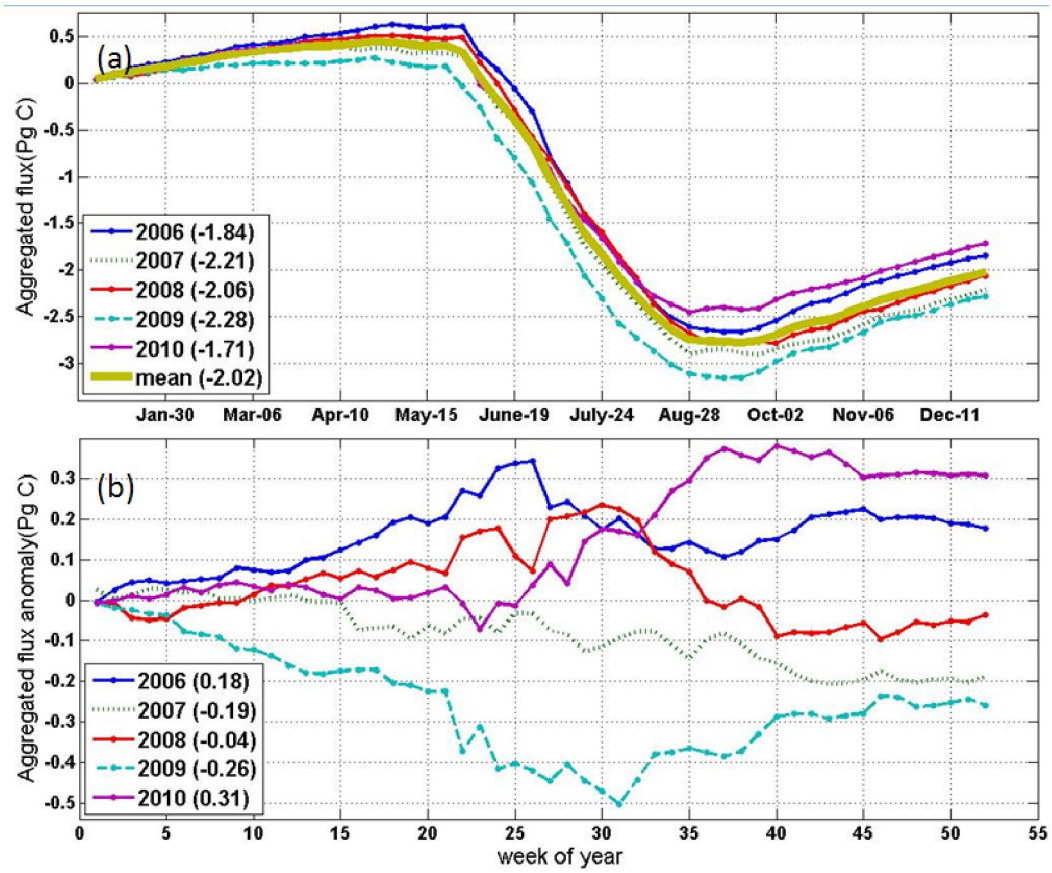

Figure 7 (a) Cumulative net ecosystem exchange (NEE) vs. time estimated in our system for each of the individual years and for the 2006-2010 mean. This figure reveals the largest uptake in 2009 and the smallest uptake in 2010. (b) Cumulative anomaly of CO_2 exchange through the year 2006-2010. The fluxes shown here include only respiration and photosynthesis, because the biomass burning emissions have a large inter-annual variability

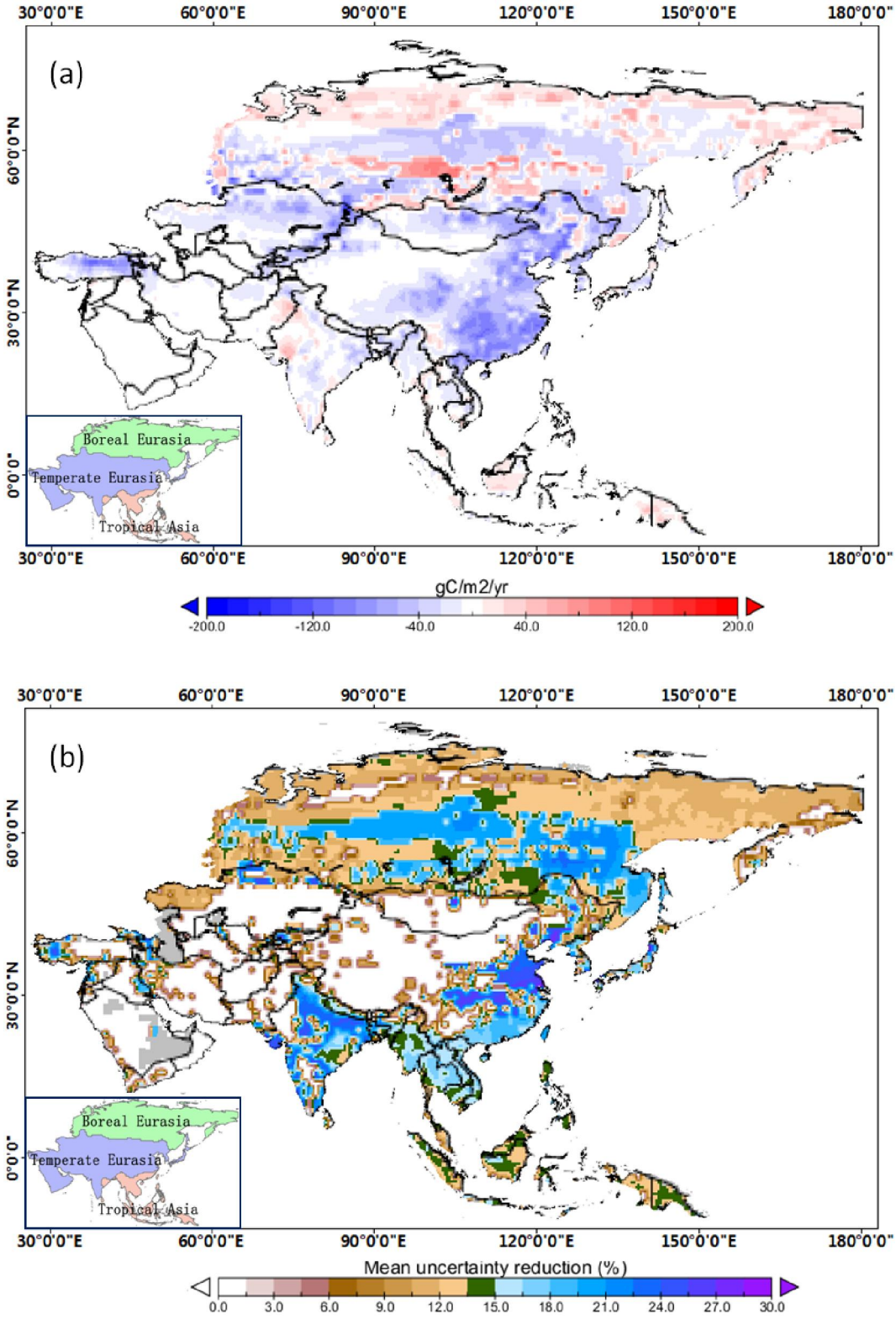

Figure 8 (a) The inverted flux difference between surface CO_2 observation data only surface (Surface-Only) and both the surface CO_2 observation data and CONTRAIL data (Surface-CONTRAIL); and (b) the Gaussian error reduction rate

between Surface-Only and Surface-CONTRAIL during 2006-2010. The flux difference is derived from: (Surface-CONTRAIL – Surface-Only), while the Gaussian error reduction rate is calculated as:

$$(\sigma_{Surface-Only} - \sigma_{Surface-CONTRAIL}) / \sigma_{Surface-Only} \times 100$$

Supporting Information Appendix A:

Table A1 Summary of the global surface CO_2 observation data assimilated between January 1, 2006 and December 31, 2010. The frequency of continuous data is one data point per day (when available), while discrete surface data point is generally once per week. MDM (model-data-mismatch) is a value assigned to a given site that is meant to quantify our expected ability to simulate observations and used to calculate the innovation X^2 (Inn. X^2) statistic. N denotes that the number is available in the CTDAS. Flagged observations mean the model-minus-observation difference if it exceeds 3 times of the model-data-mismatch and therefore is excluded from assimilation. The bias is the average from posterior residuals (assimilated values – measured values), while the modeled bias is the average from prior residuals (modeled values – measured values). Laboratory abbreviations refer to the description of the GLOBALVIEW product (Masarie and Tans, 1995).

Site	Name	Lat, Lon, Elev.	Lab	N(flagged)	MDM	Inn. X^2	Bias(modeled)
'abp_01d0'	Arembepe, Bahia, Brazil	12.77°S,38.17°W,1m	ESRL	102(0)	3	0.3	-1.18(-1.51)
'abp_26d0'	Arembepe, Bahia, Brazil	12.77°S,38.17°W,1m	IPEN	101(0)	3	0.38	-1.33(-1.67)
'alt_01d0'	Alert, Nunavut, Canada	82.45°N,62.51°W,200m	ESRL	246(0)	1.5	0.43	0.01(0.12)
'alt_06c0'	Alert, Nunavut, Canada	82.45°N,62.51°W,200m	EC	1590(0)	2.5	0.21	0.18(0.27)
'amt_01c3'	Argyle, Maine, United States	45.03°N,68.68°W,50m	ESRL	1571(59)	3	0.98	0.8(0.83)
'amt_01d0'	Argyle, Maine, United States	45.03°N,68.68°W,50m	ESRL	126(0)	1000	0	-0.11(0.14)
'amt_01p0'	Argyle, Maine, United States	45.03°N,68.68°W,50m	ESRL	307(0)	1000	0	0.69(0.52)
asc_01d1'	Ascension Island, United Kingdom	7.92°S,14.42°W,54m	ESRL	413(2)	0.75	0.91	-0.09(-0.14)
'ask_01d0'	Assekrem, Algeria	23.18°N,5.42°E,2728m	ESRL	221(0)	1.5	0.34	-0.11(-0.12)
'azr_01d0'	Terceira Island, Azores, Portugal	38.77°N,27.38°W,40m	ESRL	136(3)	1.5	0.96	0.36(0.39)
'bal_01d0'	Baltic Sea, Poland	55.35°N,17.22°E,3m	ESRL	473(0)	7.5	0.38	0.11(0.23)
'bao_01c3'	Boulder Atmospheric Observatory, Colorado, United States	40.05°N,105.00°W,1584m	ESRL	1482(42)	3	1.02	-0.46(0.11)
'bao_01p0'	Boulder Atmospheric Observatory, Colorado, United States	40.05°N,105.00°W,1584m	ESRL	760(0)	1000	0	-1.78(-1.47)
'bhd_01d0'	Baring Head Station, New Zealand	41.41°S,174.87°E,85m	ESRL	82(0)	1.5	0.3	0.09(0.09)
'bkt_01d0'	Bukit Kototabang, Indonesia	N,100.32°E,864m	ESRL	172(0)	7.5	0.73	5.53(5.51)
'bme_01d0'	St. Davids Head, Bermuda,	32.37°N,64.65°W,30m	ESRL	47(0)	1.5	0.75	0.17(0.21)

	United Kingdom						
'bmw_01d0'	Tudor Hill, Bermuda, United Kingdom	32.27°N,64.88°W,30m	ESRL	143(3)	1.5	0.69	0.19(0.21)
'brw_01c0'	Barrow, Alaska, United States	71.32°N,156.61°W,11m	ESRL	1319(1)	2.5	0.28	0.35(0.55)
'brw_01d0'	Barrow, Alaska, United States	71.32°N,156.61°W,11m	ESRL	227(2)	1.5	0.6	0.12(0.35)
'bsc_01d0'	Black Sea, Constanta, Romania	44.17°N,28.68°E,3m	ESRL	149(7)	7.5	1.33	-4.08(-3.85)
'cba_01d0'	Cold Bay, Alaska, United States	55.21°N,162.72°W,21m	ESRL	290(17)	1.5	1.28	-0.49(-0.42)
cdl_06c30'	Candle Lake, Saskatchewan, Canada	53.99°N,105.12°W,600m	EC	825(9)	3	0.7	0.79(1.5)
cfa_02d0'	Cape Ferguson, Queensland, Australia	19.28°S,147.06°E,2m	CSIRO	96(0)	2.5	0.43	-0.95(-1.19)
'cgo_01d0'	Cape Grim, Tasmania, Australia	40.68°S,144.69°E,94m	ESRL	156(0)	0.75	0.27	-0.06(-0.09)
'cgo_02d0'	Cape Grim, Tasmania, Australia	40.68°S,144.69°E,94m	CSIRO	154(1)	0.75	0.25	-0.12(-0.14)
'chr_01d0'	Christmas Island, Republic of Kiribati	1.70°N,157.17°W,3m	ESRL	192(0)	0.75	1.11	-0.59(-0.65)
'cri_02d0'	Cape Rama,India	15.08°N,73.83°E,60m	CSIRO	33(1)	3	1.4	-1.97(-2.11)
'crz_01d0'	Crozet Island, France	46.45°S,51.85°E,120m	ESRL	217(0)	0.75	0.2	-0.09(-0.14)
'cya_02d0'	Casey, Antarctica, Australia	66.28°S,110.52°E,51m	CSIRO	97(0)	0.75	0.32	-0.28(-0.32)
'egb_06c0'	Egbert, Ontario, Canada	44.23°N,79.78°W,251m	EC	1001(73)	3	1.28	0.88(1.33)
'eic_01d0'	Easter Island, Chile	27.15°S,109.45°W,50m	ESRL	153(0)	7.5	0.02	0.53(0.51)
'esp_06c0'	Estevan Point, British Columbia, Canada	49.38° N ,126.54°W,7m	EC	614(19)	3	0.63	-0.33(-0.25)
'etl_06c0'	East Trout Lake, Saskatchewan, Canada	54.35°N,104.98°W,492m	EC	1063(6)	3	0.51	0.22(0.75)
'fef_03c0'	Fraser, Colorado, United States	39.91°N,105.88°W,2745m	NCAR	2558(158)	3	0.85	-0.43(-0.42)
'gmi_01d0'	Mariana Islands, Guam	13.43°N,144.78°E,3m	ESRL	249(0)	1.5	0.29	-0.09(-0.11)
'gsn_61c0'	Gosan, Republic of Korea	33.15°N,126.12°E,72m	NIER	1274(109)	3	1.99	-1.01(-0.82)
'hba_01d0'	Halley Station, Antarctica, United Kingdom	75.61°S,26.21°W,30m	ESRL	205(0)	0.75	0.22	-0.21(-0.26)
'hdp_03c0'	Hidden Peak (Snowbird), Utah, United States	40.56°N,111.65°W,3351m	NCAR	2285(1)	3	0.27	-0.29(-0.28)
'hpb_01d0'	Hohenpeissenberg, Germany	47.80°N,11.01°E,985m	ESRL	208(0)	7.5	0	2.77(2.86)
'hun_01d0'	Hegyhatsal, Hungary	46.95°N,E,248m	ESRL	232(0)	7.5	0.39	0.35(0.5)
'ice_01d0'	Storhofdi, Vestmannaeyjar, Iceland	63.40°N,20.29°W,118m	ESRL	222(2)	1.5	0.7	-0.39(-0.35)
'izo_01d0'	Izana, Tenerife, Canary Islands, Spain	28.31°N,16.50° W,2372.9m	ESRL	207(0)	1.5	0.72	0.63(0.62)
'key_01d0'	Key Biscayne, Florida, United States	25.67°N,E,3m	ESRL	147(0)	2.5	0.23	-0.04(-0.02)
'kum_01d0'	Cape Kumukahi, Hawaii, United States	19.52°N,154.82°W,3m	ESRL	289(0)	1.5	0.44	-0.21(-0.21)
'kzd_01d0'	Sary Taukum, Kazakhstan	44.06°N,76.82°E,601m	ESRL	167(6)	2.5	1.16	-0.08(0.5)
'kzm_01d0'	Plateau Assy, Kazakhstan	43.25°N,77.88°E,2519m	ESRL	155(2)	2.5	0.96	0.5(0.63)
'lef_01c3'	Park Falls, Wisconsin, United	45.95°N,90.27°W,472m	ESRL	2267(55)	3	0.87	0.2(0.52)

	States						
'lef_01d0'	Park Falls, Wisconsin, United States	45.95°N,90.27°W,472m	ESRL	227(0)	1000	0	0.76(1.09)
'lef_01p0'	Park Falls, Wisconsin, United States	45.95°N,90.27°W,472m	ESRL	1341(0)	1000	0	0.11(0.41)
'llb_06c0'	Lac La Biche, Alberta, Canada	54.95°N,112.45°W,540m	EC	1206(43)	3	1	0.14(0.5)
'lln_01d0'	Lulin,Taiwan	23.47° N,120.87°E,2862m	ESRL	220(20)	7.5	0.99	2.62(2.65)
'lmp_01d0'	Lampedusa, Italy	35.52°N,12.62°E,45m	ESRL	197(0)	1.5	0.91	0.05(0.07)
'maa_02d0'	Mawson Station, Antarctica, Australia	67.62°S,E,32m	CSIRO	87(0)	0.75	0.34	-0.29(-0.32)
'mhd_01d0'	Mace Head, County Galway, Ireland	53.33°N,9.90°W,5m	ESRL	180(0)	2.5	0.18	0(0)
'mid_01d0'	Sand Island, Midway, United States	28.21°N,177.38°W,4m	ESRL	229(0)	1.5	0.74	0.22(0.22)
'mkn_01d0'	Mt. Kenya, Kenya	0.05°S,37.30°E,3897m	ESRL	74(0)	2.5	1.08	1.59(1.56)
'._01c0'	Mauna Loa, Hawaii, United States	19.54°N,155.58°W,3397m	ESRL	1420(4)	0.75	0.55	0.06(0.06)
'mlo_01d0'	Mauna Loa, Hawaii, United States	19.54°N,155.58°W,3397m	ESRL	251(0)	1.5	0.15	0.01(0.02)
'mnm_19c0'	Minamitorishima,Japan	24.29°N,153.98°E,8m	JMA	1624(0)	3	0.76	0.15(0.16)
'mqa_02d0'	Macquarie Island, Australia	54.48°S,158.97°E,12m	CSIRO	114(0)	0.75	0.3	-0.05(-0.07)
'nmb_01d0'	Gobabeb, Namibia	23.58°S,15.03°E,456m	ESRL	142(0)	2.5	0.19	-0.54(-0.58)
'nwr_01d0'	Niwot Ridge, Colorado, United States	40.05°N,105.58°W,3523m	ESRL	226(4)	1.5	0.62	0.21(0.18)
'nwr_01p0'	Niwot Ridge, Colorado, United States	40.05°N,105.58°W,3523m	ESRL	869(31)	1.5	1	0.44(0.43)
'obn_01d0'	Obninsk, Russia	55.11°N,36.60°E,183m	ESRL	68(5)	7.5	0.64	-1.51(-1.29)
'oxk_01d0'	Ochsenkopf, Germany	50.03°N,11.80°E,1022m	ESRL	139(10)	2.5	1.32	-0.18(-0.11)
'pal_01d0'	Pallas-Sammaltunturi, GAW Station, Finland	67.97°N,24.12°E,560m	ESRL	225(3)	2.5	0.74	0.06(0.32)
'poc_01d1'	Pacific Ocean, N/A	0.39°S,132.32°W,10m	ESRL	853(10)	0.75	0.79	-0.07(-0.1)
'psa_01d0'	Palmer Station, Antarctica, United States	64.92°S,64.00°W,10m	ESRL	247(0)	0.75	0.43	-0.27(-0.35)
'pta_01d0'	Point Arena, California, United States	38.95°N,123.74°W,17m	ESRL	200(0)	7.5	0.34	-2.19(-2.08)
'rpb_01d0'	Ragged Point, Barbados	13.17°N,59.43°W,45m	ESRL	227(0)	1.5	0.57	-0.15(-0.17)
'ryo_19c0'	Ryori,Japan	39.03°N,141.82°E,260m	JMA	1663(48)	3	0.9	0.46(0.69)
'sdz_01d0'	Shangdianzi, China	40.39°N,117.07°E,287m	CMA/ESRL	60(15)	3	1.18	0.15(0.18)
'sey_01d0'	Mahe Island, Seychelles	4.67°S,55.17°E,3m	ESRL	221(5)	0.75	0.77	-0.07(-0.08)
'sgp_01d0'	Southern Great Plains, Oklahoma, United States	36.80°N,97.50°W,314m	ESRL	225(13)	2.5	1.28	-0.51(-0.14)
'shm_01d0'	Shemya Island, Alaska, United States	52.72°N,174.10°E,40m	ESRL	149(0)	2.5	1.02	-0.11(-0.05)
'smo_01c0'	Tutuila, American Samoa	14.25°S,170.56°W,42m	ESRL	1598(0)	0.75	0.49	0.1(0.09)

'smo_01d0'	Tutuila, American Samoa	14.25°S,170.56°W,42m	ESRL	239(0)	1.5	0.16	-0.06(-0.09)
'snp_01c3'	Shenandoah National Park, United States	38.62°N,78.35°W,1008m	ESRL	1237(98)	3	1.5	-0.14(0.04)
'spl_03c0'	Storm Peak Laboratory (Desert Research Institute), United States	40.45°N,106.73°W,3210m	NCAR	1874(14)	3	0.62	-0.68(-0.69)
'spo_01d0'	South Pole, Antarctica, United States	89.98°S,24.80°W,2810m	ESRL	238(0)	1.5	0.04	-0.16(-0.2)
'stm_01d0'	Ocean Station M, Norway	66.00°N,2.00°E,0m	ESRL	343(3)	1.5	0.68	0.16(0.28)
'str_01p0'	Sutro Tower, San Francisco, California, United States	37.76°N,122.45°W,254m	ESRL	698(0)	1000	0	-0.27(-0.14)
'sum_01d0'	Summit, Greenland	72.58°N,38.48°W,3238m	ESRL	248(0)	1.5	0.47	0.16(0.21)
'syo_01d0'	Syowa Station, Antarctica, Japan	69.00°S,39.58°E,11m	ESRL	114(0)	0.75	0.22	-0.24(-0.28)
'tap_01d0'	Tae-ahn Peninsula, Republic of Korea	36.73°N,126.13°E,20m	ESRL	181(3)	7.5	0.6	1.82(2.13)
'tdf_01d0'	Tierra Del Fuego, Ushuaia, Argentina	54.87°S,68.48°W,20m	ESRL	117(0)	0.75	0.74	-0.36(-0.42)
'thd_01d0'	Trinidad Head, California, United States	41.05°N,124.15°W,107m	ESRL	232(21)	2.5	1.33	-1.49(-1.56)
'uta_01d0'	Wendover, Utah, United States	39.90°N,113.72°W,1320m	ESRL	220(11)	2.5	0.76	0.65(0.98)
'uum_01d0'	Ulaan Uul, Mongolia	44.45°N,111.10°E,914m	ESRL	231(5)	2.5	1.17	0.1(0.28)
'wbi_01c3'	West Branch, Iowa, United States	41.72°N,91.35°W,242m	ESRL	1801(141)	3	1.21	0.22(0.64)
'wbi_01p0'	West Branch, Iowa, United States	41.72°N,91.35°W,242m	ESRL	845(0)	1000	0	0.36(0.81)
'wgc_01c3'	Walnut Grove, California, United States	38.27°N,121.49°W,0m	ESRL	1736(132)	3	1.22	-0.59(-0.46)
'wgc_01p0'	Walnut Grove, California, United States	38.27°N,121.49°W,0m	ESRL	878(0)	1000	0	-4.55(-4.41)
'wis_01d0'	WIS Station, Negev Desert, Israel	31.13°N,34.88°E,400m	ESRL	239(1)	2.5	0.62	-0.1(-0.15)
'wkt_01c3'	Moody, Texas, United States	31.31°N,97.33°W,251m	ESRL	2124(24)	3	0.74	0.11(0.11)
'wkt_01d0'	Moody, Texas, United States	31.31°N,97.33°W,251m	ESRL	168(0)	1000	0	0.15(0.2)
'wkt_01p0'	Moody, Texas, United States	31.31°N,97.33°W,251m	ESRL	979(0)	1000	0	-0.42(-0.45)
'wlg_01d0'	Mt. Waliguan, Peoples Republic of China	36.29°N,100.90°E,3810m	CMA/ESRL	254(19)	1.5	0.83	-0.1(-0.14)
'yon_19c0'	Yonagunijima, Japan	24.47°N,123.02°E,30m	JMA	1684(3)	3	0.78	1.53(1.67)
'zep_01d0'	Ny-Alesund, Svalbard, Norway and Sweden	78.90°N,11.88°E,475m	ESRL	217(2)	1.5	0.75	0.61(0.8)

Supporting Information Appendix B:

Table B1 Global annual average aggregated fluxes for TransCom regions from our system compared to similar estimates from CT2011_oi and Peylin et al. (2013). The time span of each of these studies is indicated in the table. All units are Pg C yr^{-1}[a].

	Region Name	prior flux 2006-2010	This work 2006-2010		This work 2008-2010				CarbonTracker 2006-2010	Peylin et al. (2013) 2006-2010	Niwa et al. (2012)
			Case 1	Case 2	Case 3	Case 4	Case 5	Case 6	CT2011_oi[b]	CTE2013[c]	2006-2008
1	North American Boreal	-0.01	-0.23	-0.27	-0.25	-0.26	-0.22	-0.19	-0.21	-0.24	-
2	North American Temperate	-0.12	-0.52	-0.60	-0.63	-0.61	-0.56	-0.56	-0.37	-0.42	-
3	South American Tropical	0.02	0.15	0.12	-0.08	0.00	-0.05	0.00	0.18	0.09	-
4	South American Temperate	-0.07	0.11	0.00	-0.01	0.09	0.07	-0.03	0.08	-0.10	-
5	Northern Africa	0.06	0.06	0.05	0.08	-0.06	0.08	0.10	-0.07	0.00	-
6	Southern Africa	-0.05	0.05	0.06	0.10	-0.04	-0.02	0.05	-0.01	-0.01	-
7	Eurasia Boreal	0.03	-1.02	-0.96	-1.11	-1.25	-0.96	-0.92	-1.00	-0.93	-
8	Eurasia Temperate	-0.11	-0.68	-0.33	-0.70	-0.63	-0.44	-0.36	-0.41	-0.33	-
9	Tropical Asia	0.22	0.15	0.19	0.12	0.08	0.17	0.20	0.14	0.22	-
10	Australia	-0.11	-0.03	-0.02	-0.09	-0.12	-0.11	-0.12	-0.01	-0.06	-
11	Europe	-0.09	-0.48	-0.49	-0.50	-0.45	-0.61	-0.67	-0.51	-0.40	-
12	North Pacific Temperate	-0.50	-0.37	-0.38	-0.37	-0.37	-0.39	-0.40	-0.40	-0.41	-
13	West Pacific Tropical	0.00	0.00	0.00	-0.01	0.00	-0.01	-0.01	0.01	0.00	-
14	East Pacific Tropical	0.22	0.31	0.32	0.34	0.34	0.30	0.31	0.33	0.35	-
15	South Pacific Temperate	-0.53	-0.54	-0.62	-0.58	-0.58	-0.58	-0.52	-0.64	-0.60	-
16	Northern Ocean	-0.25	-0.25	-0.27	-0.26	-0.27	-0.25	-0.25	-0.25	-0.30	-
17	North Atlantic Temperate	-0.50	-0.40	-0.40	-0.38	-0.39	-0.46	-0.46	-0.43	-0.47	-
18	Atlantic Tropical	0.14	0.17	0.17	0.17	0.18	0.16	0.16	0.16	0.18	-
19	South Atlantic Temperate	-0.26	-0.17	-0.15	-0.13	-0.11	-0.18	-0.19	-0.18	-0.15	-
20	Southern Ocean	-0.61	-0.31	-0.28	-0.29	-0.28	-0.33	-0.33	-0.37	-0.29	-
21	Indian Tropical	0.13	0.14	0.14	0.14	0.14	0.14	0.14	0.18	0.15	-
22	Indian Temperate	-0.58	-0.66	-0.68	-0.67	-0.70	-0.67	-0.63	-0.70	-0.68	-
23	Non-optimized	0.00	0.00	0.00	0.00	0.00	0.00	0.00	0.00	0.00	-
24	Global Total	-2.99	-4.50	-4.41	-5.12	-5.30	-4.92	-4.68	-4.49	-4.44	-4.46
25	Global Land	-0.25	-2.43	-2.24	-3.07	-3.25	-2.65	-2.50	-2.20	-2.20	-2.67
26	Global Ocean	-2.74	-2.08	-2.16	-2.04	-2.05	-2.27	-2.18	-2.30	-2.24	-1.79
27	Asia (7,8,9)	0.13	-1.56	-1.09	-1.69	-1.80	-1.23	-1.08	-1.27	-1.05	-
28	NH Land (1,2,7,8,11)	-0.32	-2.93	-2.64	-3.20	-3.20	-2.79	-2.70	-2.50	-2.33	-
29	Tropical Land(3,5,9)	0.30	0.36	0.36	0.13	0.02	0.20	0.30	0.26	0.31	-
30	Southern Land (4,6,10)	-0.22	0.13	0.04	0.00	-0.07	-0.06	-0.10	0.05	-0.18	
31	NH Total (1,2,7,8,11,12,16,17)	-1.56	-3.95	-3.69	-4.21	-4.23	-3.89	-3.81	-3.58	-3.52	-
32	Tropical Total(3,5,9,13,14,18,21)	0.79	0.99	0.99	0.77	0.68	0.79	0.90	0.93	0.99	-
33	Southern Total(4,6,10,15,19,20,22)	-2.21	-1.55	-1.70	-1.67	-1.74	-1.82	-1.77	-1.85	-1.91	

[a]All the terrestrial biosphere fluxes are including land uptake and biomass burning emissions, but excluding fossil fuel emissions.

[b]CT2011_oi : this data is derived from http://carbontracker.noaa.gov

[c]CTE2013 is the result of Carbon Tracker Europe (Peters et al., 2010) as presented in Peylin et al., (2013) for the period of 2006-2010

The estimated (a posterior) global CO_2 sinks/sources across 6 sensitivity tests were presented in Table B1, and aggregated to annual mean for TransCom regions. These experiments form a range around the best estimate, given an alternative uncertainty with upper and lower limits of sensitivity tests to the assimilation system. As previous description, the Case 1 was performed the best assimilation on CO_2 source/sink and its results are used to analyze the global carbon flux. Our inverted results of annual carbon flux in Case 1 (Surface-CONTRAIL) shows that most land regions are estimated as carbon sinks, with strong sinks in the Eurasia Boreal, Eurasia Temperate, North American Temperate, North American Boreal and Europe, while Tropical Asia, South America, Africa are inferred as carbon sources (Table A1). The estimated ocean fluxes show the same tendencies as the *a priori* fluxes that East Pacific Tropical, Atlantic Tropical and Indian Tropical Oceans are carbon source, while others are CO_2 sinks. This distribution of carbon sinks/source is reasonable and quite consistent with another inversion estimate (Peylin et al. 2013).

Our best global mean CO_2 flux was estimated to be $-4.50^{-4.41}_{-5.30}$ Pg C yr^{-1} (uncertainty range derived from Cases 1-6) for the period 2006-2010, compared with the global *a priori* flux of −2.99 Pg C yr^{-1}. Note here that the biomass burning emissions (averaged +2.20 Pg C yr^{-1} during the studied period) were included in the inverted flux, but fossil fuel emissions (averaged +8.64 Pg C yr^{-1}) were excluded. For comparison, we included the annual means from Carbon Tracker Europe (Peters et al., 2010, quoted as CTE2013) derived from Peylin et al. (2013) and Carbon Tracker North America (quoted as CT2011_oi, data downloaded from http://carbontracker.noaa.gov) for the same time period and areas. The CT2011_oi

estimates the carbon flux of global terrestrial biosphere and oceans were respectively −2.20 Pg C yr^{-1} and −2.30 Pg C yr^{-1}, while the sink inferred fromCTE2013 was estimated to be −2.20 Pg C yr^{-1} on land and −2.24 Pg C yr^{-1} in the ocean. Our inferred global carbon sinks/source ($-4.50^{-4.41}_{-5.30}$ Pg C yr^{-1}) is well consistent with the CT2011_oi (−4.49 Pg C yr^{-1}) and CTE (−4.44 Pg C yr^{-1}). This consistency can be further represented in the partitioning of the NH land sinks between North America, Asia and Europe. In North America, our result ($-0.75^{-0.75}_{-0.88}$ Pg C yr^{-1}) generally agree with CTE2013 (−0.66 Pg C yr^{-1}) and CT2011_oi (−0.58 Pg C yr^{-1}). In Asia, the inverted result is $-1.56^{-1.07}_{-1.80}$ Pg C yr^{-1}, which is within uncertainty and comparable to CTE2013 (−1.05 Pg C yr^{-1}) and the CT2011_oi (−1.27 Pg C yr^{-1}). In Europe, our result ($-0.48^{-0.45}_{-0.67}$ Pg C yr^{-1}) is in the range of CT2011_oi (−0.51 Pg C yr^{-1}) and CTE2013 (−0.37 Pg C yr^{-1}).

Also, we found that the addition of CONTRAIL data creates a larger carbon sink in Temperate Asia, and in the NH land, at the expense of weak ocean uptake. This shifts the fluxes to a stronger land uptake versus weaker ocean sink, more in line with the results of Niwa et al. (2013) that there existed a stronger terrestrial uptake (−2.67 Pg C yr^{-1}) and a weaker oceans uptake (−1.79 Pg C yr^{-1}) caused by using CONTRAIL data.

Overall, our global, all-land and all-ocean estimates of the CO_2 flux in this period are reasonable.

Supporting Information Appendix C:

Table C1 The MODIS land use categories converted to the corresponded Olson, et al. (1985) land types table

	IGBP	Olson, et al. (1985)
0	Water Bodies	18 Non-optimized areas (ice, polar desert,inland seas)
1	Evergreen Needleleaf Forest	1 Conifer Forest
2	Evergreen Broadleaf Forest	5 Tropical Forest
3	Deciduous Needleleaf Forest	1 Conifer Forest
4	Deciduous Broadleaf Forest	2 Broadleaf Forest
5	Mixed Forest	3 Mixed Forest
6	Closed Shrublands	13 Shrub/Tree/Suc
7	Open Shrubland	4 Grass/Shrub
8	Woody Savannas	8 Fields/Woods/Savanna
9	Savannas	13 Shrub/Tree/Suc
10	Grasslands	4 Grass/Shrub
11	Permanent Wetlands	11 Wetland
12	Croplands	14 Crops
13	Urban and Built-up	18 Non-optimized areas (ice, polar desert,inland seas)
14	Cropland/Natural Vegetation Mosaic	14 Crops
15	Snow and Ice	18 Non-optimized areas (ice, polar desert,inland seas)
16	Barren or Sparsely Vegetated	12 Deserts

To assess the impact of land cover map on carbon flux, we used MODIS land cover data (MCD12Q1 version 051 of year 2005) in place of map of Olson et al. (1985). The MODIS land cover map was re-sampled into a 1×1 degree spatial resolution by selecting the pixels with maximum area, and then was converted into Olson et al. (1985) land types. The conversion strategy from MODIS IGBP categories into Olson et al. (1985) land classification are summarized in Table C1. The processed MODIS data are showed in Figure C1. We found that this land cover data are very different from that of Olson et al. (1985), which could produce large changes in inverted carbon flux.

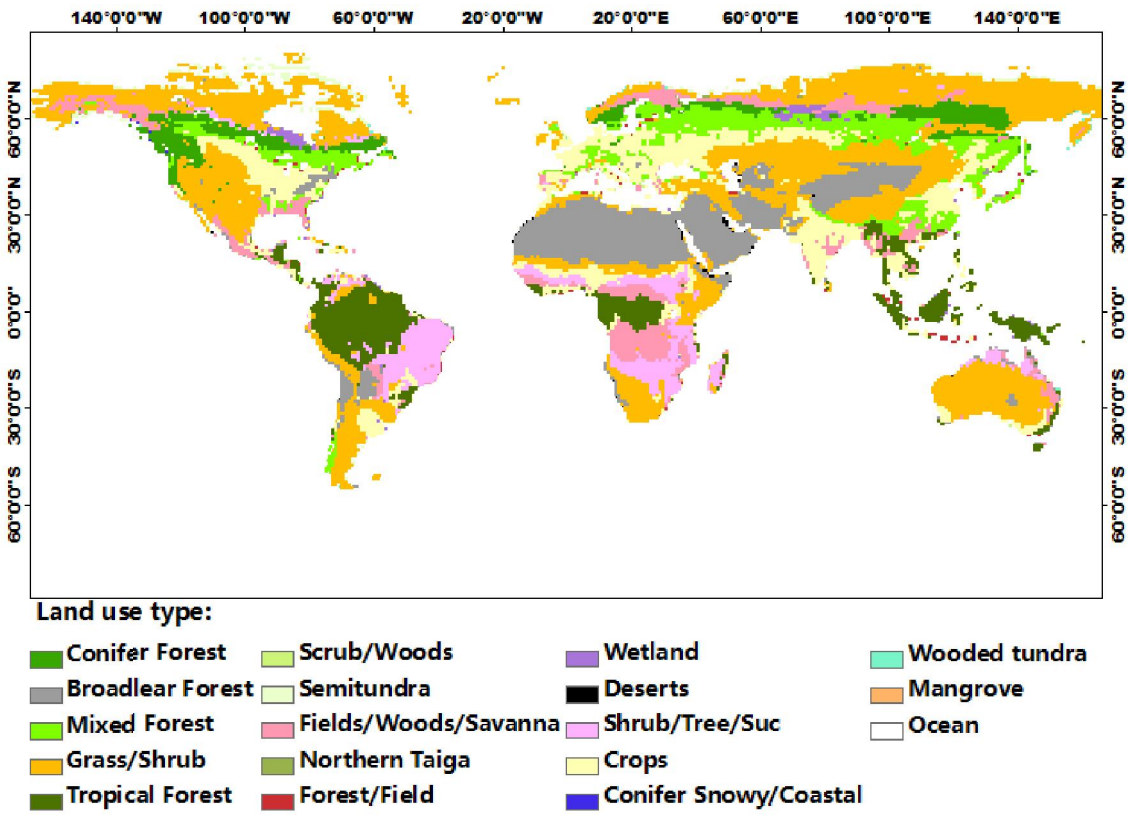

Figure C1 The land use maps (MODIS) used in Case 6